PSEUDO-NITZCHIA MULTISERIES FERRITIN IRON OXIDATION AND OXIDATIVE STRESS PROTECTION IN THE PRESENCE OF GLUTATHIONE

by

Jennifer Woolcock

B.Sc., University of Alberta, 2016

A THESIS SUBMITTED IN PARTIAL FULFILLMENT OF

THE REQUIRMENTS FOR THE DEGREE OF

MASTER OF SCIENCE

in

THE FACULTY OF GRADUATE AND POSTDOCTORAL STUDIES

(Microbiology and Immunology)

THE UNIVERSITY OF BRITISH COLUMBIA

(Vancouver)

April 2020

The following individuals certify that they have read, and recommend to the Faculty of Graduate and Postdoctoral Studies for acceptance, the thesis entitled:

PSEUDO-NITZCHIA MULTISERIES FERRITIN IRON OXIDATION AND OXIDATIVE STRESS PROTECTION IN THE PRESENCE OF GLUTATHIONE

submitted by Jennifer Woolcock in partial fulfillment of the requirements for

the degree of Master of Science

in Microbiology and Immunology

Examining Committee:

Dr. Michael Murphy, Microbiology and Immunology
Supervisor

Dr. J. Thomas Beatty, Microbiology and Immunology
Supervisory Committee Member

Dr. William Mohn, Microbiology and Immunology
Additional Examiner

Additional Supervisory Committee Members:

Dr. Sean Crowe, Microbiology and Immunology
Supervisory Committee Member

Abstract

Iron is an essential nutrient for most organisms, including diatoms. A portion of intracellular iron is attributed to the labile iron pool (LIP), which is readily exchangeable iron available to bind to enzymes to participate in biological reactions. Iron belonging to the LIP is transiently bound to cellular ligands, such as glutathione (GSH). However, iron present in the cell in excess can be toxic to the cell, as ferrous iron can react with H_2O_2 in the Fenton reaction to produce highly detrimental reactive oxygen species (ROS). *Pseudo-nitzchia multiseries* is a marine planktonic diatom that plays an important role in primary production and carbon sequestration in the ocean. *P. multiseries* expresses an iron storage protein, ferritin (PmFtn), which protects the cell from oxidative damage by oxidizing iron at ferroxidase centres and storing iron in a nano-cage formed from 24 monomers. Ferritin ferroxidase activity is poorly characterized in the presence of biologically-relevant iron chelators of the LIP. In this study, PmFtn ferroxidase activity was found to proceed at a slower rate in the presence of GSH. In a PmFtn structure obtained from a crystal soaked in the presence of iron and GSH for 30 minutes, iron was found bound to the ferroxidase centre at sites A and B, consistent with spectroscopic data showing rapid binding of iron but slow mineralization in the presence of GSH. PmFtn and GSH also protected DNA from H_2O_2 mediated oxidative stress in the presence of iron.

Lay Summary

Iron is an essential nutrient for most organisms, including marine diatoms. However, excess iron can be toxic to the cell. Iron can cause the formation of reactive oxygen species through the Fenton reaction, which can go on to cause cell death. *Pseudo-nitzchia multiseries* is a marine diatom important in photosynthesis. It produces an iron storage protein, ferritin, which allows it to inhibit the effects of the Fenton reaction by storing excess iron. The purpose of this study was to determine ferritin iron binding and storage in the presence a cellular iron chelator, GSH. The structure of ferritin revealed that iron was still able to bind the active site in the presence of GSH. However, the rate of iron binding and uptake by ferritin was much lower in the presence of GSH. Ferritin was also found to be protective of DNA when DNA was exposed to oxidative stress and excess iron.

Preface

The work in this thesis includes contributions from my fellow scientists in the Murphy Lab. The PmFtn synthetic gene construct for protein expression and crystallization was designed by Dr. Stephanie Pfaffen. The PmFtn spectroscopic function assays were modified from assays originally developed by Dr. Slade Loutet. All other work described in this thesis is my original, unpublished work.

This project required biohazard approval for the handling of *Escherichia coli*. Approval was provided by the UBC Biosafety Committee, Certificate number: B17-0242.

Table of Contents

List of Tables

List of Figures

List of Abbreviations

Bfr	Bacterioferritin
BfrB	*Pseudomonas aeruginosa* bacterioferritin
DNA	Deoxyribonucleic acid
Dps	DNA-binding protein from starved cells
EcBfr	*Escherichia coli* bacterioferritin
EcFtnA	*Escherichia coli* ferritin A
EcFtnB	*Escherichia coli* ferritin B
EDTA	Ethylenediaminetetraacetic acid
EMSA	Electrophoretic mobility shift assay
FtnA	*Pseudomonas aeruginosa* ferritin
Fur	Ferric uptake regulator
GSH	Glutathione
IPTG	Isopropyl b-D-thiogalactopyranoside
LB	Luria-Bertani
LIP	Labile iron pool
MES	2-(*N*-morpholino)ethanesulfonic acid
MOPS	3-(N-morpholino)propanesulfonic acid
*Mtb*BfrA	*Mycobacterium tuberculosis* bacterioferritin
*Mtb*BfrB	*Mycobacterium tuberculosis* ferritin
PCR	Polymerase Chain Reaction
PDB	Protein Data Bank
PmFtn	*Pseudo-nitzchia multiseries* ferritin
RMSD	Root mean square deviation
ROS	Reactive oxygen species
SDS-PAGE	Sodium dodecyl sulphate polyacrylamide gel electrophoresis
SSRL	Stanford Synchotron Radiation Lightsource

TCEP	Tris(2-carboxyethyl)phosphine

Acknowledgments

I would like to express my gratitude towards Dr. Michael Murphy, who gave me the chance to conduct research and learn new skills in his lab as a Masters student. I will be forever grateful for the support and guidance Dr. Murphy has offered me throughout the years that I have been fortunate enough to be a part of his lab. I also would like to extend my gratitude to my committee members, Dr. J. Thomas Beatty and Dr. Sean Crowe for providing helpful feedback and advice on my research.

I would like to sincerely thank all past and present members of the Murphy Lab for all of their advice, mentorship, and friendship. To Angelé, thank you for all of your help and patience in learning new lab techniques, and for keeping things running smoothly in the lab. To Anson and Angela, thank you for providing all of your expertise in learning everything there is to know about crystallography. To Daniela, thank you for your help in making my figures look pretty in R. To Brigid, thank you for being my dear friend in the lab, and for always offering me your kindness and support.

Finally, I would like to thank my friends and family for all of their love and support over the past few years. To Dorothy, for being my roommate and good friend during this unique time in my life, and for listening to all the triumphs and tribulations that came with it. To my mom and dad, I can never thank you enough for always being there for me and believing in me every step of the way.

Chapter 1: Introduction

1.1 Iron in biology

Iron is one of the most abundant transition metals found on Earth. It is an essential nutrient required by all eukaryotes, as well as for most prokaryotes and archaea. Iron acts as a key cofactor in numerous biological processes, including but not limited to cellular respiration, photosynthesis, DNA synthesis, and biocatalytic transformations (1). The Fe^{2+}/Fe^{3+} redox pair possess a wide range of physiologically relevant reduction potentials, from approximately -500 to +600 mV depending on the environment in which it is found. The ease in gaining and losing an electron allows iron to participate in oxidation-reduction reactions and activate oxygen (2). Iron is found in cells associated with proteins as mononuclear or binuclear iron, or as part of more complex iron-sulfur clusters or heme groups (3,4).

Primitive life experienced an Earth which contained low levels of dioxygen. This allowed for ferrous iron (Fe^{2+}) to be readily available for use by cells. Later, the evolution of photosynthesis caused a surge of dioxygen, which led to the predominant form of iron on the Earth's surface becoming the oxidized and relatively insoluble ferric (Fe^{3+}) form (5). The decrease in solubility and bioavailability of iron resulted in iron becoming a limiting nutrient for many organisms in the present day. Iron not only presents a challenge to the organisms that are dependent on it by being commonly found in its insoluble ferric form, but additionally, soluble ferrous iron in the presence of H_2O_2 can react inside the cell to form hydroxyl radicals. This phenomenon is called the Fenton reaction, and can be illustrated by a chemical equation (equation 1) (6,7).

$$Fe\ (II) + H_2O_2 \rightarrow Fe\ (III) + OH^- + {}^{\cdot}OH \qquad (1)$$

The Fenton reaction creates a problem for the cell that is two-fold: firstly, it reduces iron bioavailability, as ferrous iron is oxidized by H_2O_2 to the relatively insoluble ferric form, and secondly, the hydroxyl radicals produced from this reaction can go on to damage DNA and other cellular components, and can ultimately result in cell death (6). As such, microorganisms have developed numerous strategies to limit the effects of the Fenton reaction.

1.2 The labile iron pool

The labile iron pool (LIP) describes iron ions which are free to participate as a cofactor in biological reactions (8). This comprises a small percentage of cellular iron, however, data on the specific content of metals in microbial cells is limited. The best data exist for *Escherichia coli*, with a total iron cellular iron content of ~200 µM, 10-30 µM of which is attributed to the LIP (62). In general, the iron attributed to the LIP for most microorganisms is thought to be under 5% of total cellular iron under normal cellular conditions (50-100 µM). The amount of iron in the LIP is proposed to be maintained homeostatically for cells to meet the metabolic demands for iron, while also minimizing the potential for ROS formation via the Fenton reaction (8). This is achieved using the ferric uptake regulator (Fur) system in bacterial cells (64). The term LIP is often referred as is “free iron”. This is a misnomer, as most of this iron is in the ferrous form transiently bound to cellular ligands, such as organic anions, polypeptides, and surface components of membranes (8). As such, a more appropriate broader definition for the iron pool is iron belonging to chemical forms which can potentially be bound by enzymes to participate in cellular redox reactions or scavenged by strong iron chelators (8,9). Ligands that bind iron in the LIP include sulfhydryl-containing metabolites, such as glutathione and cysteine. These metabolites are able to bind ferrous iron rapidly, and are crucial in preventing iron from creating detrimental free hydroxyl radicals through the Fenton reaction (10, 13). As such, damage to these

metabolites via oxidative stress can be further detrimental to the cell, as ferrous iron is then released, and is therefore free to participate in hydroxyl radical formation via the Fenton reaction (7).

1.2.1 Glutathione

Glutathione (GSH) is a low molecular-weight thiol found in high abundance in cells, estimated at an average of between 3-10 mM in the cell, but can be sometimes found at even higher concentrations (10). GSH is a tripeptide which contains a N-terminal glutamic acid, a C-terminal glycine, and a central cysteine (Figure 1-1). The main biosynthetic pathway for GSH is the γ-glutamyl cycle, in which L-glutamic acid is joined to L-cysteine in an ATP-dependent reaction catalyzed by glutamate cysteine ligase. Glycine is then added to γ-Glu-Cys by forming an amide bond with the cysteine carboxyl group in a second ATP-dependent reaction catalyzed by glutathione synthase (11). Cysteine is the most limited in availability, and so is the limiting precursor of this reaction. *De novo* synthesis aside, the most important mechanism the cell employs to maintain the cellular concentration of GSH is the reduction of glutathione disulfide by glutathione reductase using NADPH (11).

GSH plays many important functions within the cell. It plays a role in disulphide bond reduction in conjunction with the thioredoxin pathway. GSH is also an important redox buffer in cells, which reduces oxidized cysteine residues as well as protects them from irreversible oxidation (10). In most organisms, including diatoms, GSH is the most abundant low molecular weight thiol antioxidant present in the cell. As such, GSH is critical in maintaining thiol–disulfide balance and detoxifying H_2O_2 via the ascorbate–GSH cycle within diatom cells (12). The ascorbate-GSH cycle involves ascorbate peroxidase using two molecules of ascorbate to reduce H_2O_2 to water, followed by the generation of two molecules of monodehydroascorbate, a

radical which is reduced to ascorbate. However, some monodehydroascorbate also rapidly disproportionates to dehydroascorbate before it can be reduced. Dehydroascorbate is subsequently reduced to ascorbate by dehydroascorbate reductase, using GSH as the reducing substrate. This reaction generates glutathione disulphide, which is in turn re-reduced to GSH by NADPH, a reaction catalyzed by glutathione reductase (65, 66). GSH also plays a major role in iron metabolism in the cell. The binding affinity of Fe^{2+} for GSH is a log K_1 value of 5.1, and $GS{\cdot}Fe^{2+}$ is predicted to be the dominant cytoplasmic Fe^{2+} species, followed by hexaaquo$\cdot Fe^{2+}$ (13). GSH possesses a buffering role for cytoplasmic Fe^{2+} and offers a means for the selection of iron for its subsequent incorporation into a wide range of iron-dependent enzymes and electron transfer proteins (13).

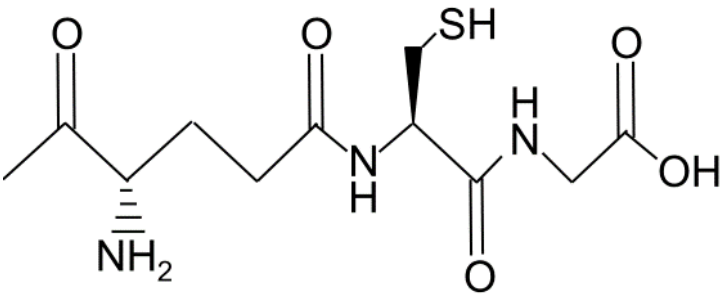

Figure 1-1. Chemical structure of glutathione.

1.3 Marine diatoms

Among the most diverse members of the phytoplankton communities in the world's oceans are diatoms, which comprise an estimated 200,000 different species. They are unicellular, photosynthetic organisms which belong to the Stramenopiles. These organisms are believed to

have arisen from a secondary endosymbiotic event, in which an ancestral protist engulfed a red and a green alga (12). As a major component of marine phytoplankton, diatoms play an important role in photosynthesis and primary production in the world's oceans (14). In addition, diatoms have a major influence on the global geochemical cycles of several nutrients, including carbon, nitrogen, and silica (15).

Diatoms are diverse, with members ranging greatly in size, morphology, and lifestyle. There are both the centric diatoms, which have a round morphology, and the pennate diatoms, which appear more elongated in their morphology (15, 16). Diatoms use diverse strategies to meet cellular iron demands, including the use of high-affinity iron uptake systems, iron storage proteins, substitutions of iron-requiring proteins with proteins which do not require iron, and enzymes to mitigate the risk of reactive oxygen species produced by excess cellular ferrous iron (14).

Pseudo-nitzschia multiseries is a pennate marine diatom, and an important player in primary production and carbon sequestration in the oceans. As photosynthetic organisms, they require additional iron, with about half of that iron being contained in their photosynthetic proteins (16, 18). *P. multiseries* has adapted to the limitation of iron in the environment by using ferritins to store iron within their cells (19). It is likely through use of these iron storage proteins that *P. multiseries* is able to become the numerically dominant planktonic species in diatom blooms stemming from iron fertilization in the ocean, which can occur either from upwelling of iron from the deep ocean, or by deposition of continental dust or volcanic activity (19, 20).

1.4 Ferritins

The ferritin-like superfamily of proteins is characterized by 4-helix bundle fold (Figure 1-2). Ferritins and bacterioferritins, a heme-containing variant ferritin protein found in some prokaryotes, form large 24-subunit spherical nanocage proteins with the capability to store iron within a hollow core of about 80 Å in diameter (21, 22, 23). The subunits of these proteins are composed of four α-helix bundles, with a fifth shorter α-helix at the C-terminus. The B and C helices are connected by long loops, which allows them to be parallel to one another. The 24 subunits are arranged in a highly symmetric way, with a dimer of subunits forming each face of the nanocage, and with an octahedral 432 point-group symmetry (29). Both ferritins and bacterioferritins are described as having iron storage capability, as well as playing a possible role in iron detoxification within cells (21). These proteins oxidize ferrous iron to the ferric form and can store up to 4500 iron ions as a ferrihydrate mineral within their central cavity (22, 23). Ferritin nanocages contain channels which connect the inner cavity to the external environment, and when iron is required by the cell, iron is subsequently reduced and released from the ferrihydrite mineral core of the protein (24). In some bacterial species, a ferritin with 12 subunits are found and are referred to as a "mini-ferritin". These mini-ferritins store less iron in their relatively smaller inner cavities. Mini-ferritins are described as being DNA-binding proteins from starved cells (Dps) (22).

The ferroxidase centre of ferritin is where ferrous iron binds to the protein, is subsequently oxidized, and migrates to the mineral core, a process referred to as iron mineralization (Figure 1-2) (25). Each of the 24 subunits of the ferritin protein contain a ferroxidase centre, comprising of typically 2 or 3 iron-binding sites each, depending on the species. Most eukaryotic ferroxidase centres contain only 2 iron-binding sites, while prokaryotic

and archaeal ferroxidase centres may contain a third iron-binding site (26, 27). The ferroxidase centres of the proteins tend to be highly conserved. Of the five key residues which coordinate iron in eukaryotic H chain ferritins (Glu, Glu, Glu, His, Gln), four are conserved in prokaryotic ferritins (Figure 1-3) (28). Despite structural similarity amongst members of this super-family of proteins, there is little amino acid sequence identity between members of this group outside of conservation of the residues which form the ferroxidase centres. Amino acid sequence identity between ferritins from different species averages ~15% (30).

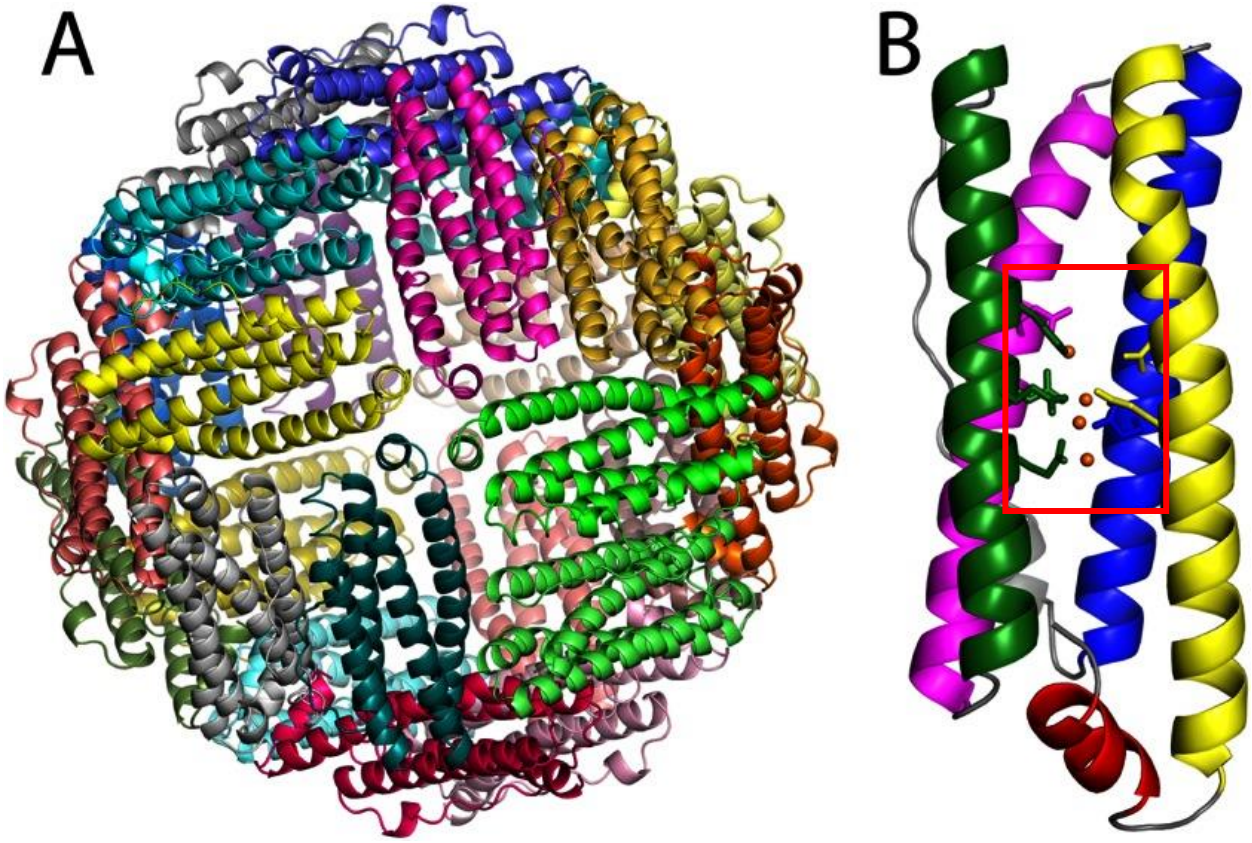

Figure 1-2. Crystal structure of PmFtn. (A) Crystal structure of the recombinant iron-soaked *P. multiseries* ferritin multimer (PDB ID: 4IWK), showing the typical ferritin structure with 24 subunits forming a spherical shell with a hollow core. (B) A PmFtn monomer showing the ferroxidase centre containing three iron-binding sites within the red box, as well as a fourth proximal iron-binding site. Side chains are represented as stick models, with bound iron atoms represented by orange spheres. Figure adapted with permission from (31).

1.4.1 Microbial ferritins

Ferritins have been isolated and characterized from a wide range of bacterial species, as well as from a small number of thermophilic archaea. Ferritins may be distinguished from bacterioferritins by not being associated with any heme groups. In some prokaryotic and archaeal ferritins, the ferroxidase centres contains a third proximal iron-binding site, site C, though its exact role remains unclear from species to species (32). In some organisms, site C may play a role in iron movement to the core for mineralization, and in other organisms it likely plays a role in iron oxidation alongside iron-binding sites A and B. This third iron-binding site distinguishes prokaryotic and archaeal ferritins from mammalian ferritins and bacterioferritins (33).

Interestingly, a single organism can possess genes for more than one member of this superfamily of proteins, despite their roles being seemingly redundant. For example, *Escherichia coli* possess genes for two ferritins (EcFtnA and EcFtnB), a bacterioferritin (EcBfr), and a Dps protein (34). Studying these proteins in *E. coli* has indicated that EcFtnA plays a major role in iron storage within the cell, and that Dps plays a role in protecting the cell from oxidative stress. However, the exact roles for EcFtnB and EcBfr remain unclear. In contrast, *Pseudomonas aeruginosa* possesses genes for one ferritin (FtnA) and one bacterioferritin (BfrB), but in the case of *P. aeruginosa*, BfrB is believed to the main iron storage protein, with the role of FtnA remaining unknown (35). Organisms which have one or more genes from the ferritin-like superfamily of proteins deleted from their genome often exhibit failure to thrive under growth conditions of both iron deficiency and oxidative stress (34).

1.4.2 Diatom ferritins

Diatoms are believed to have acquired ferritins through lateral gene transfer from cyanobacteria (19). Ferritin proteins are found in all diatom lineages, although they are mostly absent from the centric diatoms. They share a similar structure to ferritins from other domains of life, and form a large hollow sphere made up of 24 identical subunits (Figure 1-2). Little sequence similarity is observed when compared to prokaryotic, mammalian, or archaeal ferritins except at the ferroxidase centres, where the residues which coordinate iron are well-conserved (36).

Pseudo-nitzchia multiseries, a marine pennate diatom, possess a gene encoding ferritin (PmFtn) in its genome, and the recombinant ferritin is well-characterized (19, 31, 36). *P. multiseries* is not known to possess genes for any additional ferritin proteins. Like prokaryotic ferritins, PmFtn contains 3 iron-binding sites at its ferroxidase centre, including a site C which is located closer to the mineral core (Figure 1-3). This was the first eukaryotic ferritin discovered to contain a third iron site. Contrary to the function of site C in prokaryotic and archaeal ferritins, iron-binding site C in PmFtn is unlikely to be involved in iron oxidation, and instead likely acts as a transit site for iron to migrate towards the inner core of the protein (36). PmFtn also possesses signal peptide and plastid transit peptide motifs to target ferritin subunits to the plastid. The plastid is where ferritin likely plays a role in storing iron and preventing formation of ROS, as well as delivering iron for iron-requiring processes, such as photosynthesis (19).

1.4.3 Bacterioferritins

Bacterioferritins are members of the ferritin-like superfamily of proteins that are found exclusively in prokaryotes, and have been isolated from a wide variety of bacterial species.

These proteins share key residues with ferritins at their di-iron ferroxidase centres (Figure 1-3) (37). A distinguishing feature of bacterioferritins is the presence of 12 heme groups bound to their protein structure, which are absent in other ferritin proteins. These heme groups are located at the junctions between two subunits, and were shown to not serve a function in iron uptake at the ferroxidase centres, as heme-free variants of bacterioferritin were not affected in iron mineralization (29, 37, 38). Instead, heme associated with bacterioferritin may play a role in iron release from the inner cavity (39).

1.4.4 Dps

Besides the 24-subunit ferritins, there is also a sub-family of ferritins composed of only 12 subunits, termed "mini-ferritins", that are isolated only in prokaryotes and archaea (40). DNA-binding protein from starved cells (Dps) is a mini-ferritin that contains 12 catalytic ferroxidase centres located at each of the six faces of the dodecameric protein. These centres are formed at the interface of two subunits, each with a high-affinity iron-binding site A and low-affinity iron-binding site B (30). Some Dps proteins bind to DNA non-specifically, forming stable and highly-organized Dps-DNA complexes that protect DNA from H_2O_2 during stationary phase. Though it was originally speculated that Dps achieved DNA protection through a mechanism of physical shielding, it is now believed that Dps provides bimodal protection of DNA (30). Unlike other ferritins, ferrous irons bound to ferroxidase centres of Dps are mainly oxidized by H_2O_2, and are comparatively inefficiently oxidized using O_2. This iron oxidation process also contributes to the observed Dps protection of the cell against oxidative stress, as Dps activity helps to prevent the formation of hydroxyl radicals via the Fenton reaction by reducing H_2O_2 (30). The lysine-containing N-terminus of Dps was found to be a crucial element in Dps-DNA co-crystallization and in Dps self-aggregation. (30). While the function of Dps is

mainly focused on its DNA-protection abilities, Dps also exhibits the characteristic iron storage capacity shared by all members of the ferritin super-family of proteins.

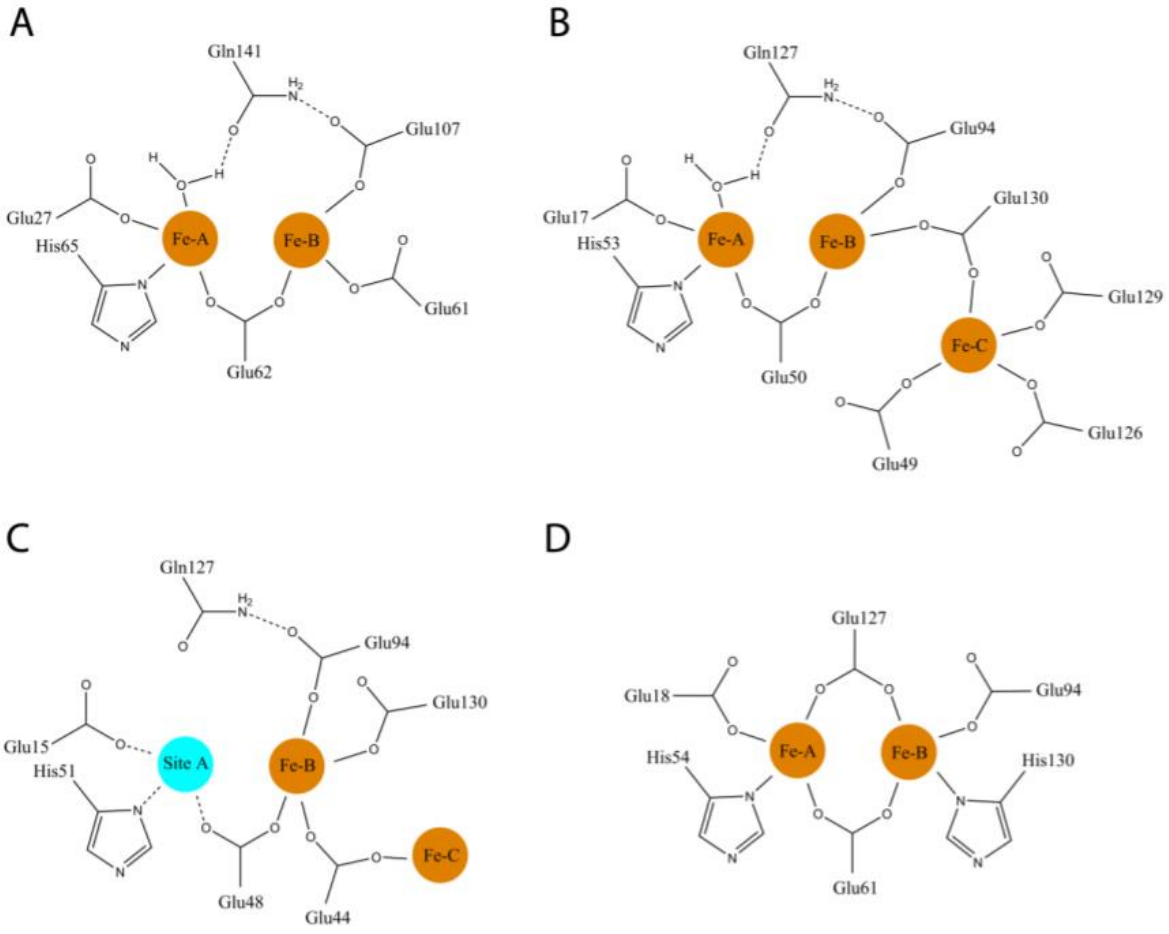

Figure 1-3: Ferroxidase centres of ferritins. Covalent and metal-ligand bonds are drawn as solid lines. Hydrogen bonds are drawn as dotted lines. (A) Ferroxidase centre of human H-chain ferritin. (B) Ferroxidase centre of *E. coli* FtnA, including third iron binding site C. (C) Ferroxidase centre of *Pseudo-nitzschia multiseries* ferritin with a water molecule was modeled into site A. (D) Ferroxidase centre of *E. coli* bacterioferritin. Figure adapted with permission from (41).

1.5 Mechanism for iron storage

Two main competing models of ferroxidase function currently exist in the literature. The first model hypothesizes that the ferroxidase centre functions as a substrate site, where two ferrous iron molecules bind and are then oxidized by O_2 to become Fe^{3+}-O(H)-Fe^{3+} (42). This ferric hydroxide then spontaneously migrates to the mineral core of ferritin as a unit (Figure 1-4). The second model for ferritin ferroxidase function is that a sequential displacement of Fe^{3+} by Fe^{2+} is what drives the migration of ferric iron to the core of the protein (Figure 1-4). This theory postulates that in the absence of any free ferrous iron, Fe^{3+} is stuck at the ferroxidase centre and therefore unable to migrate to the core of the protein (33).

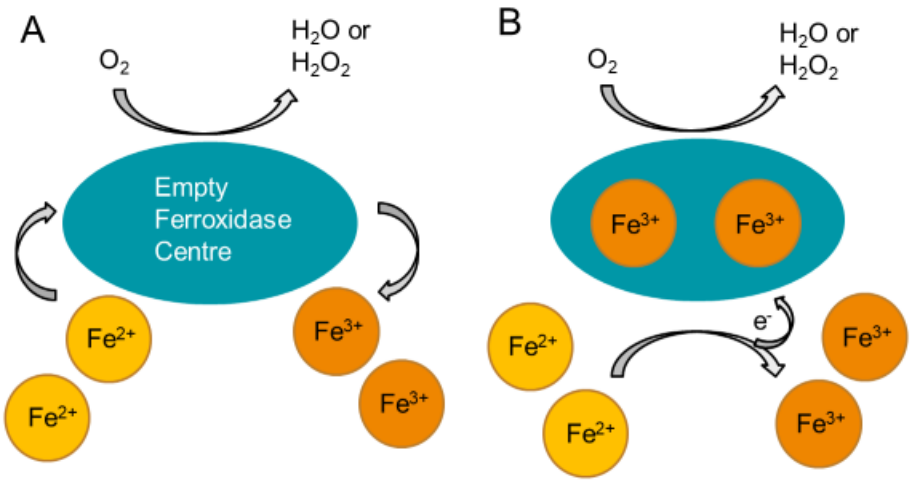

Figure 1-4. Two models for iron mineralization at the ferritin ferroxidase centre. (A) The ferroxidase centre acts as a substrate where ferrous iron is oxidized and then moves to the mineral core of the protein. (B) The ferroxidase centre acts as a cofactor, where iron ions bound there cycle between reduced and oxidized forms, first oxidized by oxygen, and then subsequently reduced by electrons transferred from ferrous iron ions that bind in the central cavity. Figure adapted with permission from (41)

1.5.1 The diatom ferroxidase centre

PmFtn contains three iron-binding sites at its ferroxidase centre, termed sites A, B and C (Figure 1-4). Iron in site A is coordinated by two glutamate residues (Glu15 and Glu48), as well as a weaker interaction with a histidine (His51). Site B contains three conserved glutamate residues (Glu48, Glu94, Glu130), as well as one that is unique to PmFtn (Glu44) (31). Iron bound in site C is coordinated by only one ligand, Glu44. Site C is likely important in moving iron towards the inner cavity of the protein (Figure 1-4). The PmFtn ferroxidase centre exhibits a characteristic two-step process when oxidizing iron: first, there is an extremely rapid initial binding and oxidation of iron (31). In this step iron saturates the PmFtn iron-binding sites A and B and is oxidized. In terms of the 24-mer nanocage, this step results in the binding and oxidation of 48 iron ions. A subsequent oxidation of additional iron occurs at a slower rate and is referred to as the mineralization rate.

Previous experiments involving PmFtn crystals soaked in the presence of dioxygen and ferrous iron for 10 minutes resulted in the presence of iron bound at sites B and C only, while site A was instead occupied by a water molecule. PmFtn crystals soaked in the presence of dioxygen and ferrous iron for 4 or more hours had iron bound at all 3 sites, as well as at a fourth proximal binding site thought to be involved in nucleation and formation of the iron mineral core. However, in the absence of dioxygen, PmFtn crystals soaked for up to 2 hours with ferrous iron had iron bound exclusively at site A at an occupancy of ~50% (31). These structures support a model with a step-wise binding mode of ferrous iron and dioxygen to the PmFtn ferroxidase centre. First, a ferrous iron binds to PmFtn site A, followed by the binding of a dioxygen or another oxidant. Only after this second step can ferrous iron then bind to site B. Ferrous iron

binding at site B is also proposed to be the rate-determining step for iron oxidation by PmFtn (31).

1.6 Antioxidant properties of ferritin

While Dps has been canonically described as the main member of the ferritin-like superfamily of proteins able to protect DNA from oxidative damage, other members of this protein super-family are proposed to also play a significant role in preventing oxidative damage to the cell (30). Ferritins possess iron detoxification properties by being able to bind, oxidize, and store iron, thus preventing iron from reacting with H_2O_2 and producing reactive oxygen species (ROS) via the Fenton reaction. In addition, ferritins can also detoxify H_2O_2 directly by utilizing it as a co-substrate along with O_2 at the ferroxidase centres during the formation of the ferrihydrite mineral core.

Dps has been singled out as the main ferritin protein which protects DNA from oxidative stress due to its ability to bind and form stable complexes with DNA, offering a more direct physical protection of DNA from oxidative stress. However, some ferritins bind DNA, thus offering physical protection of DNA from oxidative damage in a similar manner to Dps. For example, the bacterium *Mycobacterium tuberculosis* lacks a gene encoding for Dps, but encodes a gene for both bacterioferritin (*Mtb*BfrA) and a ferritin (*Mtb*BfrB). *Mtb*BfrA was shown to bind DNA based on electrophoretic mobility shift binding assays, as well as to protect DNA from degradation when exposed to oxidative stress (43). These findings indicate that Dps proteins are not alone in their ability to protect DNA amongst members of the ferritin-like superfamily of proteins, and also points towards further redundancy of the function of these proteins.

1.7 Objectives

Iron is an essential nutrient for almost all organisms, and genes for members of the ferritin-like superfamily of proteins are widespread in organisms across all three domains of life. Organisms which have one or more genes from the ferritin-like superfamily of proteins deleted from their genome often exhibit failure to thrive under conditions of oxidative stress (24). It is therefore of vital importance to better understand the roles of these proteins and the roles in which they play that allow cells to thrive.

To date, ferritin function is largely ascribed to iron storage. Though ferritins are suggested to play a role in iron detoxification in the cell, alternate roles outside of iron storage for this protein are poorly investigated. Importantly, biochemical assays of ferritin ferroxidase function are performed in simple buffer salts lacking biologically-relevant iron-chelating metabolites, and thus may not reflect function under true cellular conditions. I hypothesize that ferrous iron in the cell is chelated by sulfhydryl-containing metabolites such as GSH, and the presence of these metabolites impact ferritin function.

In this study I defined PmFtn function in the presence of GSH using spectrophotometric assays. I determined that the presence of GSH affected oxidation of iron by PmFtn. I investigated iron binding at the ferroxidase centre in the presence of sulfhydryl-containing metabolites using crystallographic methods, and determined that iron was able to bind to PmFtn ferroxidase centres in the presence of GSH and cysteine. I also tested the ability of PmFtn to protect DNA from oxidative stress, and observed that while PmFtn does not bind DNA directly as its mode of protection, PmFtn was able to prevent DNA degradation when it was incubated with DNA prior to H_2O_2 exposure.

Chapter 2: Methods

2.1 Bacterial strains and growth conditions

Bacterial strains used in this work are listed in Table 2-1. *E. coli* cultures were grown in Luria-Bertani (LB) broth or on LB-agar. Growth medium was supplemented with kanamycin (25 μg/mL) when appropriate.

Table 2-1 Bacterial strains used in this study.

Bacterial Strain	Description	Source
E. coli DH5α	Strain used for general cloning. Inserts are highly stable due to recA1 mutation. High DNA yields and quality due to endA mutation.	Life Technologies
E. coli BL21(DE3)	Strain used for protein overexpression. Contains a chromosomal copy of the phage T7 RNA polymerase gene inducible by IPTG. Deficient in lon and ompT proteases.	Novagen

2.2 PmFtn plasmid transformation

Plasmids used in this work are listed in Table 2-2. A gene encoding recombinant PmFtn (residues 1 to 168) was synthesized and confirmed by sequencing (GeneWiz Inc). The gene encodes for recombinant PmFtn protein lacking the signal peptide and plastid transit motifs from the N-terminus, with the substitutions C77V, C111V, C163V to allow for protein crystallization without the need to covalently modify the cysteine residues by an additional iodoacetamide treatment step (31). Plasmid purified from DH5α cells was transformed into *E. coli* BL21(DE3) cells by electroporation for recombinant protein expression.

Table 2-2. Plasmids used in this study.

Plasmid	Description	Source
pET28a (+)	*E. coli* cloning and protein expression vector. Contains a strong T7*lac* promoter, an optimized RBS, a multiple cloning site, and a kanamycin resistance gene.	Novagen
pET28a-PmFtnSynGene	pET28a (+) containing a construct for recombinant expression of the synthetic PmFtn gene.	This study
pET28a-ArnDLEHHH107A	pET28a (+) containing a construct for recombinant expression of mutant ArnD	GenScript

2.3 Recombinant expression and purification of PmFtn protein

PmFtn recombinant protein was overexpressed in *E. coli* BL21(DE3) cells. LB media (1 L) supplemented with 25 µg/mL kanamycin was inoculated with ~5 mL of overnight culture and incubated at 37 °C with shaking for 2-3 hours until an OD600 of ~0.8 was reached. Protein expression was induced with 1 mM isopropyl β-D-thiogalactopyranoside (IPTG) and the cultures were incubated overnight at 25 °C with shaking at 200 rpm. Cells were harvested by centrifugation at 5,000 x g for 10 minutes and resuspended on ice in lysis buffer (20 mM Tris-HCl pH 8.0, 5% glycerol (v/v), 1 mM TCEP, 5 mM EDTA, 1 M NaCl), supplemented with 100 µL protease inhibitor cocktail (Thermo Fisher Scientific) and DNase. Cells were lysed at 4°C with an EmulsiFlex-C5 homogenizer (Avestin) and insoluble material was pelleted by centrifugation at 10,000-15,000 x g for approximately 1 hour.

Soluble material was aliquoted into 2 ml centrifuge tubes and heat-shocked in a dry heat block for 10 mins at 60 °C to precipitate *E. coli* proteins. Tubes were transferred onto ice for 10

min. afterwards. Insoluble material was spun down in a microfuge, and soluble material was pooled. Polyethyleneimine (w/v) solution (10%) was added to soluble material and gently shaken on ice for 15 min. to remove any remaining DNA contamination. The solution was aliquoted into 2 ml centrifuge tubes and insoluble material was spun down in a centrifuge. Supernatant was collected and dialyzed in Source Q Buffer A (20 mM Tris-HCl pH 8.0, 5% glycerol (v/v), 1 mM TCEP, 5 mM EDTA) overnight at 4°C.

Soluble lysate was filtered with a 0.45 µm syringe filter. Protein was applied to a Source 15Q ion exchange column. A linear gradient of 0-0.5 M NaCl buffer was used to elute protein off of the column. Fractions containing ferritin protein were confirmed and purity was assessed by running them on an SDS-PAGE gel. Fractions containing protein were then dialyzed in iron-stripping buffer (3% sodium dithionite (w/v), 1 M sodium acetate, 1 mM TCEP), titrated to pH 4.8 using acetic acid, for 4 hours at 4 °C make apo-PmFtn. Protein was then exchanged into storage buffer (50 mM MES pH 6.5, 5% glycerol (v/v), 100 mM NaCl, 1 mM TCEP) by dialysis overnight at 4 °C. Finally, protein was concentrated in an Amicon and stored at -70 °C. Protein concentrations were measured using predicted extinction coefficients (25230 M^{-1} cm^{-1}) at 280 nm calculated by the ExPASy ProtParam tool (https://www.expasy.org/) based on primary amino acid sequences.

2.4 PmFtn function spectroscopic assays

In a plastic cuvette with a final volume of 1 ml, purified apo-PmFtn was added to a final concentration of 0.1 µM, and GSH was added to a final concentration of 15 mM to buffer (50 mM MES pH 6.5, 100 mM NaCl) and mixed by inverting 3X. This solution was blanked at 310 nm on a Cary-Win UV spectrophotometer. A fresh solution of ammonium ferrous sulfate was prepared in acidified milliQ water (1 µl 12 M HCl per 1 ml milliQ water) and added to the

experimental cuvette last to a final concentration of 50 µM, and was mixed by inverting 3X. To observe iron oxidation in the presence of PmFtn and GSH, absorbance of the solution was measured at 310 nm every 10 sec. for 30 min. on the spectrophotometer.

Ferrozine was added to quantify the amount of ferrous iron remaining at the end of the reaction. Ferrozine is a colorimetric indicator, which binds ferrous iron exclusively to form a purple complex which can be measured at an absorbance of 562 nm (41). Following the 30-min. reaction, the spectrophotometer was blanked at 562 nm with a solution containing buffer (50 mM MES pH 6.5, 100 mM NaCl) and 15 mM GSH, and 100 µL of a 4 mM ferrozine solution, to a total final volume of 1.1 ml. For each experimental reaction, 100 µL of 4 mM ferrozine solution was added, mixed by inverting 3X, and the absorbance measured at 562 nm.

The order in which reagents were added to the experimental cuvette was altered. GSH (15 mM) and 50 µM of freshly-prepared ammonium ferrous sulfate were added to buffer (50 mM MES pH 6.5, 100 mM NaCl) in a plastic cuvette, mixed by inverting 3X, and blanked at 310 nm. Apo-PmFtn (0.1 µM) was added to the cuvette last, mixed by inverting 3X, and absorbance was read at 310 nm every 10 sec. for 30 min. on the spectrophotometer. At the end of the 30-min. assay, residual ferrous iron was assayed using ferrozine as described previously.

To determine if GSH inhibits ferroxidation by PmFtn, 0.1 µM of apo-PmFtn in MES buffer was blanked at 310 nm before the addition of 50 µM of freshly-prepared ammonium ferrous sulfate. Absorbance at 310 nm was measured every 10 sec. for 5 min. on the spectrophotometer to observe iron oxidation. After 5 min., GSH to 15 mM was added and mixed by inverting 3X. Absorbance at 310 nm was measured every 10 sec. for a further 25 min. At the end of the 30-min. assay, the residual concentration of ferrous iron was measured using ferrozine.

2.5 Stopped-flow absorbance spectroscopy

To better understand the initial rapid binding and oxidation of iron at PmFtn ferroxidase centres in the presence of GSH, the reaction was monitored using stopped-flow absorbance spectroscopy. All stopped-flow experiments were carried out at the University of East Anglia by the Le Brun laboratory. Purified apo-PmFtn was mixed with between 6-96 Fe^{2+} equivalents, and GSH. Apo-PmFtn mixed with 96 Fe^{2+} ions in the absence of any GSH was used as a control. Absorbance at 340 nm was recorded over the course of 10 seconds to observe initial iron oxidation by PmFtn.

2.6 Crystallization and structure determination of PmFtn

Apo-PmFtn was crystallized using sitting-drop vapour diffusion at room temperature. The reservoir contained 0.1 M sodium acetate, pH 5.5, 1-1.2 M ammonium sulfate, and 0.9-1.2 M sodium chloride. Crystals formed in a 4-µL drop containing a 1:1 mixture of 15 mg/mL apo-PmFtn in buffer (50 mM MES pH 6.5, 5% glycerol (v/v), 100 mM NaCl, 1 mM TCEP) and reservoir solution. The crystals used to collect the X-ray datasets for structure solution were cryoprotected in reservoir solution supplemented with 30% glycerol, and then were flash frozen in liquid nitrogen. Diffraction data was collected at the Stanford Synchrotron Radiation Lightsource (SSRL). The data were processed and scaled using XDS (42). All crystals were of space group P4 with twelve molecules in the asymmetric unit. The molecular replacement model was prepared using the Phenix suite with a previously determined structure of PmFtn (PDB ID: 4IWK). The molecular replacement phases were determined using Phaser-MR and a preliminary model was generated using AutoBuild, both programs from the Phenix suite (43, 44, 45, 46). Manual building was performed in Coot, and refinement was carried out with phenix.refine. PyMOL (Version 1.7, Schrödinger, LLC) was used to produce structure figures (47).

Crystals were soaked in mother liquor supplemented with 2 mM of freshly prepared ammonium ferrous sulfate alone, 2 mM ammonium ferrous sulfate and 15 mM GSH, or 2 mM ammonium ferrous sulfate and 2.5 mM cysteine. Crystals were soaked aerobically in their respective solutions for 30 minutes. Crystals were then submerged in a cryoprotectant (mother liquor supplemented with 30% glycerol) before being flash-frozen in liquid nitrogen. As a control, apo-Pmftn crystals not soaked were also sent for data collection.

Diffraction data was collected at the Stanford Synchotron Radiation Lightsource (SSRL). The data were processed and scaled using XDS. All crystals were of space group *P*4 with twelve molecules in the asymmetric unit. The molecular replacement model was prepared using the Phenix suite with the structure of native PmFtn obtained from this study, which had been modified to have no loops. The molecular replacement phases were determined using Phaser-MR. Manual building was performed in Coot, and refinement was carried out with phenix.refine. PyMOL (Version 1.7, Schrödinger, LLC) was used to produce structure figures. For each of the soaking conditions, iron was modelled into iron-binding sites A and B for each of the molecules in the asymmetric unit, resulting in up to 24 Fe^{3+} ions modelled per PmFtn crystal. The presence of Fe^{3+} ions was confirmed using the anomalous map and iron occupancies were refined in Phenix.

2.7 Protection of DNA against oxidative damage

The DNA protection ability of PmFtn was tested using a linear DNA construct. The ArnD gene chosen, and was amplified from a plasmid (Table 2-1) using Phusion enzyme and T7 primers (Thermofisher) for PCR. The PCR product was verified on a 1.5% (w/v) agarose DNA gel and purified using a PCR cleanup kit (Qiagen). 15 ng/µL of linear DNA was incubated with 1.6 µM apo-PmFtn 24-mer protein for 30 minutes in 100 mM MOPS buffer, pH 7.0. To determine if the presence of GSH affected linear DNA protection from oxidative stress, samples were incubated with 1 mM GSH for 5 minutes. Samples were then incubated with 100 µM freshly-prepared ammonium ferrous sulfate for a further 10 minutes. Finally, samples were exposed to oxidative stress by being incubated for 5 minutes with 4.5 mM H_2O_2. Following incubation, samples were run for 30 minutes at 100 V on a 1.5% (w/v) agarose gel in TAE buffer and stained using SybrSafe. Gels were visualized using a UV gel imager.

Chapter 3: Results

3.1 Structure of PmFtn

To better understand iron binding at the PmFtn ferroxidase centres in the presence of iron-chelating sulfhydryl-containing metabolites, the structure of PmFtn was solved under soaking conditions with ferrous iron and cysteine or GSH. A previously solved structure of PmFtn (PDB ID: 4WIK) was used for phasing by molecular replacement (31). All crystals analyzed crystallized into the space group P4, with 12 molecules in the asymmetric unit. Data collection and refinement statistics for the highest quality crystal for each condition are summarized in Table 3-1. All PmFtn structures were determined to a resolution between 1.46-1.76 Å, and each structure had >98% of residues in the most favoured regions of the Ramachandran Plot (Table 1-3).

All the structures shared the typical ferritin fold, with 24 subunits coming together to form a large hollow spherical shell. Individual protamers were made up of a four-helix bundle along with a shorter C-terminal α-helix. A superimposition was performed in PYMOL between monomer A from the PmFtn 30-min. iron-soaked structure from this study, and monomer A from a PmFtn 45-min. iron-soaked structure from a previous study (PDB ID: 4WIJ) (31). The RMSD value with no outlier rejection between the two structures was 0.69 Å among 159 C-α positions, confirming that the PmFtn structure obtained in this study is similar to that obtained previously.

The anomalous dispersion signal was used to determine the presence of transition metals within the ferroxidase centres of each structure. In the case of apo-PmFtn, no significant peaks in an anomalous electron density map were detected in any of the ferroxidase centres. Water was modelled into these sites instead, according to positive density found in *Fo-Fc* difference maps.

Iron was initially modelled into ferroxidase centres for each of the different soaking conditions using the anomalous map generated from the anomalous signal, and then occupancies were refined in Phenix. Addition of iron or iron plus a chelator in soaks did not significantly change the protein structure compared to apo-PmFtn, except at the ferroxidase centres. Electron density maps of iron modelled into ferroxidase centres of PmFtn for each of the soaking conditions are shown in Figure 3-1. The maps obtained show that this method can be used effectively to monitor iron binding at the ferroxidase centre under different soaking conditions.

Table 3-1. Data collection and refinement statistics for PmFtn*

	Apo-PmFtn	PmFtn + Fe	PmFtn + GSH + Fe	PmFtn + Cys + Fe
Data Collection				
Resolution Range (Å)	39.98 – 1.76	39.09 – 1.76	40.03 – 1.64	40.00 - 1.46
Space Group	P4	P4	P4	P4
Unit cell dimensions (Å)	123.23, 123.23, 173. 09	123.57, 123.57, 173.42	123.38, 123.38, 173.51	123.28, 123.28, 173.49
Unique Reflections	495733 (36131)	491733 (32951)	610369 (45002)	863854 (62299)
Completeness (%)	99.7 (96.9)	95.6 (87.5)	97.3 (96.9)	97.3 (94.7)
Average $I/\sigma I$	16.87 (2.47)	15.93 (2.83)	11.12 (1.64)	12.01 (1.48)
R_{meas}	5.5 (53.1)	5.4 (45.4)	7.1 (68.9)	5.6 (70.2)
CC ½	99.9 (79.6)	99.9 (84.3)	99.8 (64.4)	99.9 (67.3)
Wilson B Factor ($Å^2$)	28.97	30.99	29.77	27.39
Refinement				
R_{work} (R_{free})	0.1623 (0.1952)	0.1607(0.1954)	0.1666(0.1954)	0.1491(0.1658)
r.m.s.d. Bond Length (Å)	0.018	0.013	0.017	0.006
Average *B*-values ($Å^2$)	22.99	24.14	25.71	24.65
Ramachandran Plot (%)				
- Most favoured regions	98.6	98.6	98.7	99.2
- Disallowed regions	0.0	0.05	0.05	0.0

*Values in parentheses are for data in the highest resolution shell

3.2 Iron binds PmFtn ferroxidase centres in the presence of GSH and cysteine

Apo-PmFTN crystals were soaked aerobically in the presence of freshly-prepared 2 mM ammonium ferrous sulfate for 30 minutes to observe the binding of iron at ferroxidase centres. Two crystals from this soaking condition were examined, each refined to a resolution of at least 1.8 Å. Iron ions were found exclusively in iron-binding sites A and B for each of the protein monomers based on inspection of the anomalous density map. Iron-binding site C was not occupied by iron, consistent with previous observations that iron occupied all three iron-binding sites after iron soaks of 4 or more hours (31). However, this result differs from the previous study, which observed iron binding at site A only after an iron-soaking time of 45 min. (31). Here, the iron occupancy at site A was at an average of 46% over the 12 monomers in the asymmetric unit, while the occupancy for site B was at an average of 50%. The range of iron occupancy at the ferroxidase site was 30 to 70%, consistent with previous observations that a soaking time of under an hour resulted in partial occupancy (31) (Figure 3-2).

Iron binding at the ferroxidase centres in the presence of a biologically-relevant iron chelator was tested next. Apo-PmFtn crystals were soaked aerobically in the presence of 2 mM of ammonium ferrous sulfate and 15 mM of GSH for 30 minutes, or in the presence of 2 mM of ammonium ferrous sulfate and 2.5 mM L-cysteine for 30 minutes. 2 crystals from each soaking condition were examined, with each crystal refined to a resolution of at least 1.8 Å. Iron ions were found exclusively in iron-binding sites A and B for each of the protein monomers in both cases (Figure 3-1). Iron-binding site C was not occupied by iron ions.

In the case of the iron and GSH soaking experiments, the average iron occupancy was not significantly different between sites A and B based on a paired 2-sample t-test with an α-value of 0.05. The iron occupancy at site A was an average 38%, while the iron occupancy for site B was

an average of 42%. In one monomer of the asymmetric unit, iron was not modelled in the ferroxidase site at all based on the anomalous signal. The presence of GSH caused a significantly lower iron occupancy on average at both iron-binding sites A and B when compared to the iron-only soaked PmFtn crystals based on a paired 2-sample t-test with an α-value of 0.05 (Figure 3-2).

In the case of the iron and cysteine soaks, the average iron occupancies between sites A and B were found to not be significantly different, with iron occupancy at site A at 40%, and iron occupancy for site B at an average of 47%. Similar to the Fe-only soak and the GSH and Fe soak, iron occupancy in site A was on average lower than in site B. Iron-binding at sites A and B was found to not be significantly different when compared to the Fe-only soak. However, the presence of cysteine resulted in significantly higher iron occupancy at iron-binding site A, but not at site B, than what was observed for the iron and GSH soaked crystals based on a paired 2-sample t-test with an α-value of 0.05 (Figure 3-2).

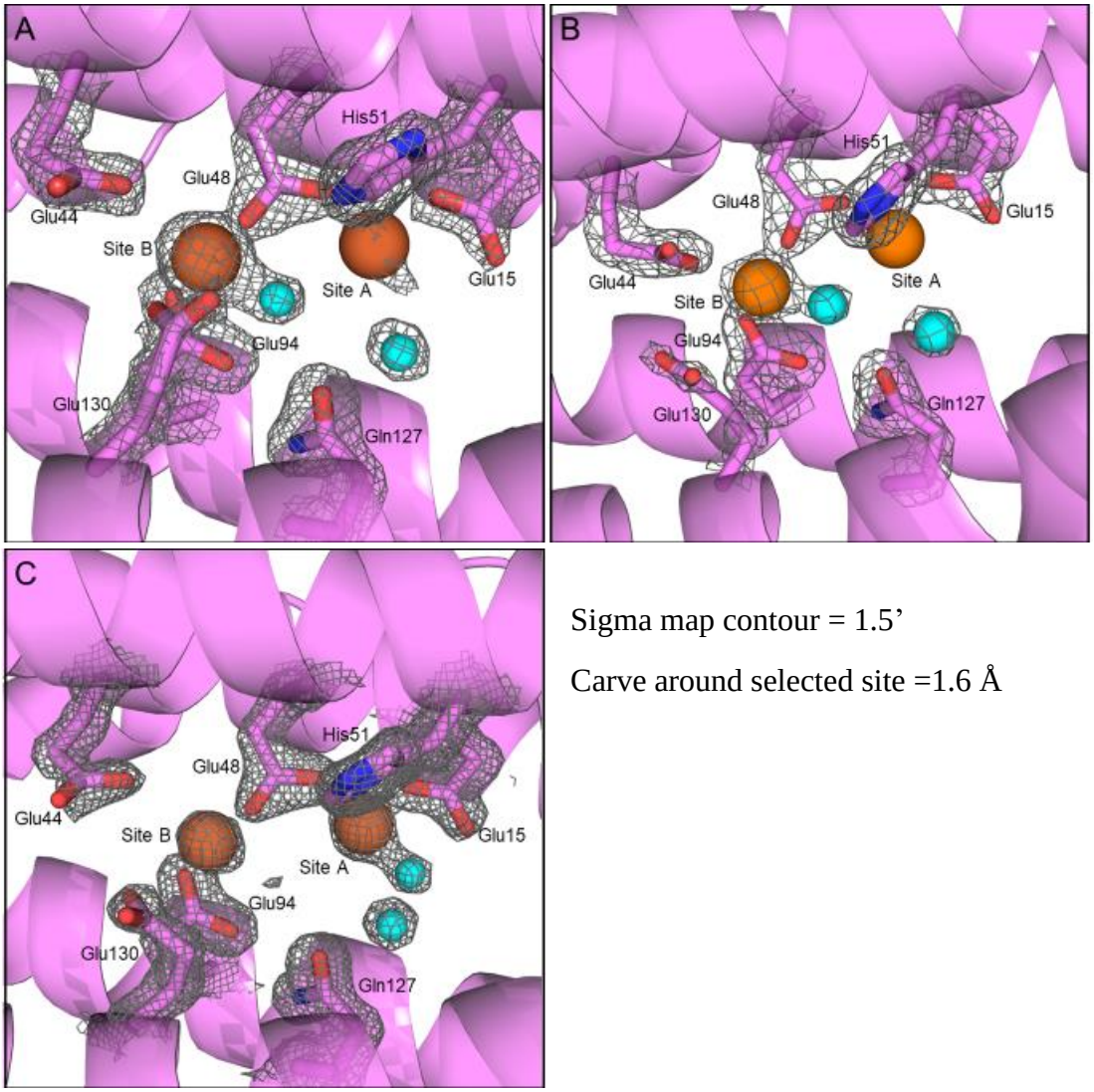

Sigma map contour = 1.5’

Carve around selected site =1.6 Å

Figure 3-1. Iron bound at PmFtn iron-binding sites A and B. Apo-PmFtn crystals were soaked in the presence of 2 mM ammonium ferrous sulfate alone, or with an iron chelator (15 mM GSH or 2.5 mM cysteine). Iron was modelled into the crystal structure based on the anomalous signal. Iron ions are represented by orange spheres, water molecules are represented by cyan spheres. A) Apo-PmFtn was soaked in the presence of ammonium ferrous sulfate, B) Apo-PmFtn soaked in the presence of ammonium ferrous sulfate and GSH, and C) Apo-PmFtn soaked in the presence of ammonium ferrous sulfate and cysteine.

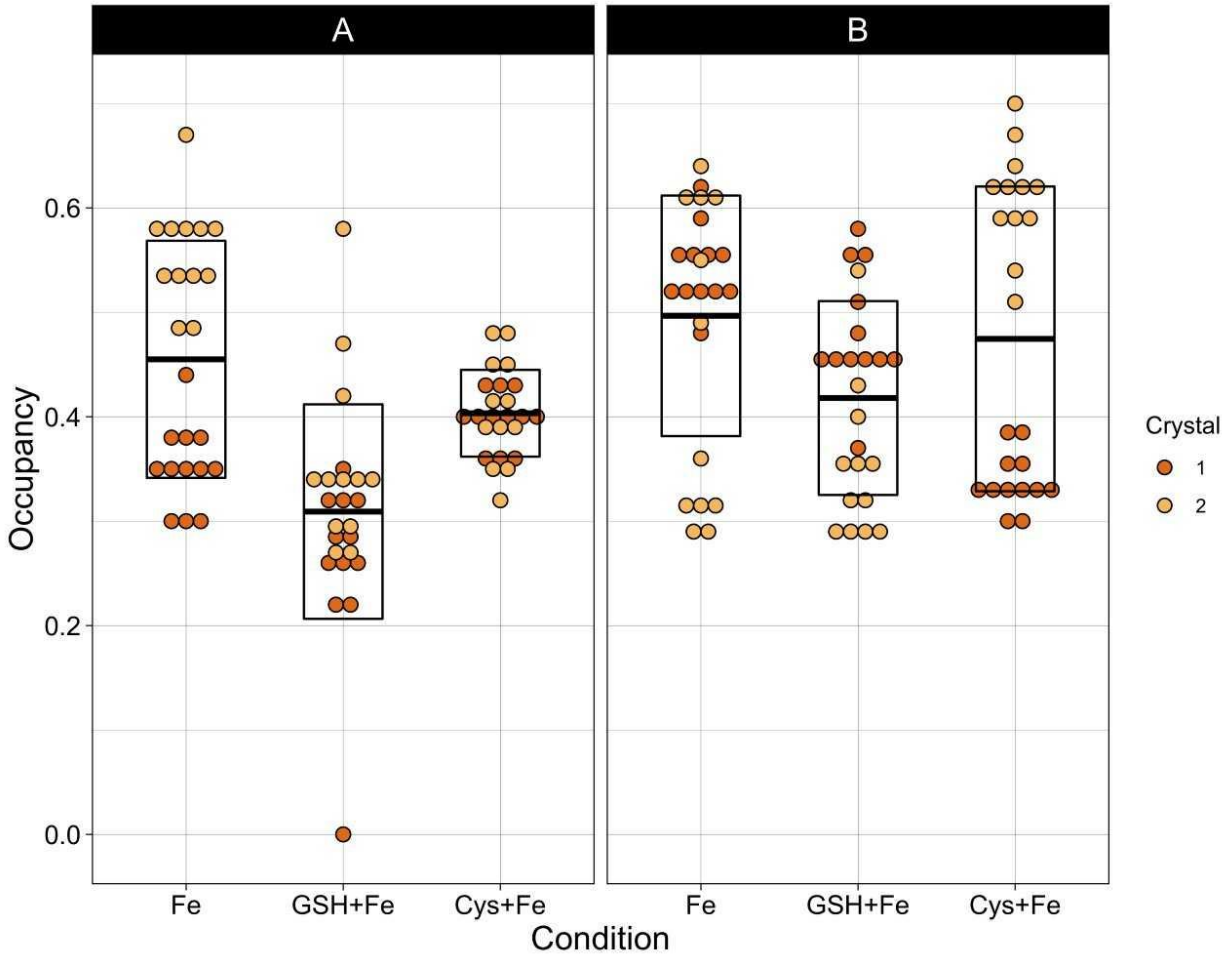

Figure 3-2. Iron occupancies at iron-binding sites A and B in PmFtn crystal structures after 30-minute soaks. Apo-PmFtn crystals were grown at room temperature. Crystals were soaked for 30 minutes in solutions containing either 2 mM ammonium ferrous sulfate, 2 mM ammonium ferrous sulfate + 2.5 mM cysteine, or 2 mM ammonium ferrous sulfate + 15 mM GSH. Iron was modelled into crystal structures and occupancies refined for all 3 conditions. Values for iron occupancies are represented by the orange and yellow dots. Iron occupancies were recorded at iron-binding sites A and B of 12 subunits (the asymmetric unit) for 2 crystals (crystal 1 = orange, crystal 2 = yellow) for each crystal condition. The line in the boxes represent the mean of the occupancies, and the boxes represent 1 standard deviation of error from the mean.

3.3 GSH inhibits iron oxidation and mineralization by PmFtn

To observe if the presence of a biologically-relevant iron chelator could inhibit either the initial rapid binding and oxidation of ferrous iron by PmFtn, or prevent the subsequent oxidation and mineralization, iron oxidation by PmFtn was assayed in the presence of GSH using spectrophotometry. A classic steady-state ferroxidase assay was performed, where iron oxidation and mineralization by PmFtn was measured at an absorbance of 310 nm. In the absence of any iron-chelating metabolites, a steady rate of iron oxidation and mineralization was observed over the course of 30 minutes (Figure 3-3). The rate is comparable to that previously observed for steady-state PmFtn iron oxidation (31). The first absorbance readings at 310 nm were greater than baseline likely due to the extremely rapid first step of PmFtn ferroxidase function, which involves the initial binding and oxidation of two ferrous iron ions at iron-binding sites A and B. This step is likely faster than the mixing time in this experiment.

Next, PmFtn ferroxidase function was tested in the presence of GSH. Oxidation and mineralization of iron was observed at a much lower rate in the presence of GSH at a biologically-relevant concentration compared to that of the ferroxidase assay in buffer (Figure 3-3). Initial absorbance at 310 nm was above baseline, consistent with a rapid initial phase of iron oxidation; however, the initial absorbance was lower compared to the control assay in the absence of GSH.

The order in which reagents are added in the assay altered the observed ferroxidase reaction. When GSH and ammonium ferrous sulfate were mixed together first, and PmFtn was added to the cuvette last, the initial absorbance was much lower than that observed when ammonium ferrous sulfate was added last. Also, iron oxidation proceeded over the course of the 30 minutes at a slower rate than in the control ferroxidase assay (Figure 3-3). The data suggest

that when ferrous iron is added last, PmFtn and GSH compete for free ion. When ferrous iron is incubated with GSH, the rate limiting step of the ferroxidase reaction may be iron release for GSH.

The effect of the addition of GSH on iron oxidation by PmFtn was examined. A ferroxidase assay in the absence of an iron chelator was monitored for five minutes, followed by the addition of GSH to 15 mM, and the assay was continued for a further 25 minutes. In the absence of GSH, the rate of iron oxidation and mineralization was similar to the control assay. After the addition of GSH, the ferroxidase rate first slowed and then was not detectable (Figure 3-3). These results indicate that GSH inhibits iron oxidation and mineralization by PmFtn, likely by iron chelation.

Ferrous iron was detected at the end of the 30-minute reaction using a ferrozine assay. In the control ferroxidase function assay in the absence of any iron chelators, < 5 μM of ferrous iron was detected at the end of the 30-minute reaction (Figure 3-4). This indicated that > 90% of ferrous iron was oxidized by PmFtn during the assay, as was expected. When ammonium ferrous sulfate was mixed with both PmFtn and GSH, an average of ~53 μM ferrous iron was detected at the end of the 30-minute reaction (Figure 3-4). The measured concentration is slightly higher than the initial 50 μM of ammonium ferrous sulfate that went into the reaction, possibly due to the reductive activity of GSH. A control of ammonium ferrous sulfate mixed alone in buffer was measured at the end of 30-minutes to account for any spontaneous oxidation of iron under aerobic conditions. Little to no iron oxidation was detected for this control, with an average of ~50 μM of ferrous iron detected at the end of the 30 minutes, corresponding to the initial concentration of ferrous iron in the reaction (Figure 3-4). Another control was performed which measured iron oxidation at the end of 30 minutes when ammonium ferrous sulfate was in the

presence of GSH alone. The results yielded ferrous iron concentrations with an average of ~55 μM (Figure 3-4) consistent with GSH as a minor source interference in the assay.

The order in which reagents were added in the reaction also resulted in a difference in remaining ferrous iron concentration at the end of the reaction. When GSH and PmFtn were mixed first in buffer, and ammonium ferrous sulfate was added last, PmFtn and GSH had equal opportunity to bind iron, which resulted in consumption of 20% of the ferrous iron, indicating that PmFtn was able to oxidize some of the ferrous iron present (Figure 3-4). In contrast, when GSH and ammonium ferrous sulfate were mixed first in buffer, and PmFtn was added last, ~50 μM remained (Figure 3-4). GSH chelates ferrous iron preventing PmFtn from oxidizing and storing the majority of iron present at the end of the 30 min reaction. These results together indicate that there is competition between GSH and PmFtn for iron binding.

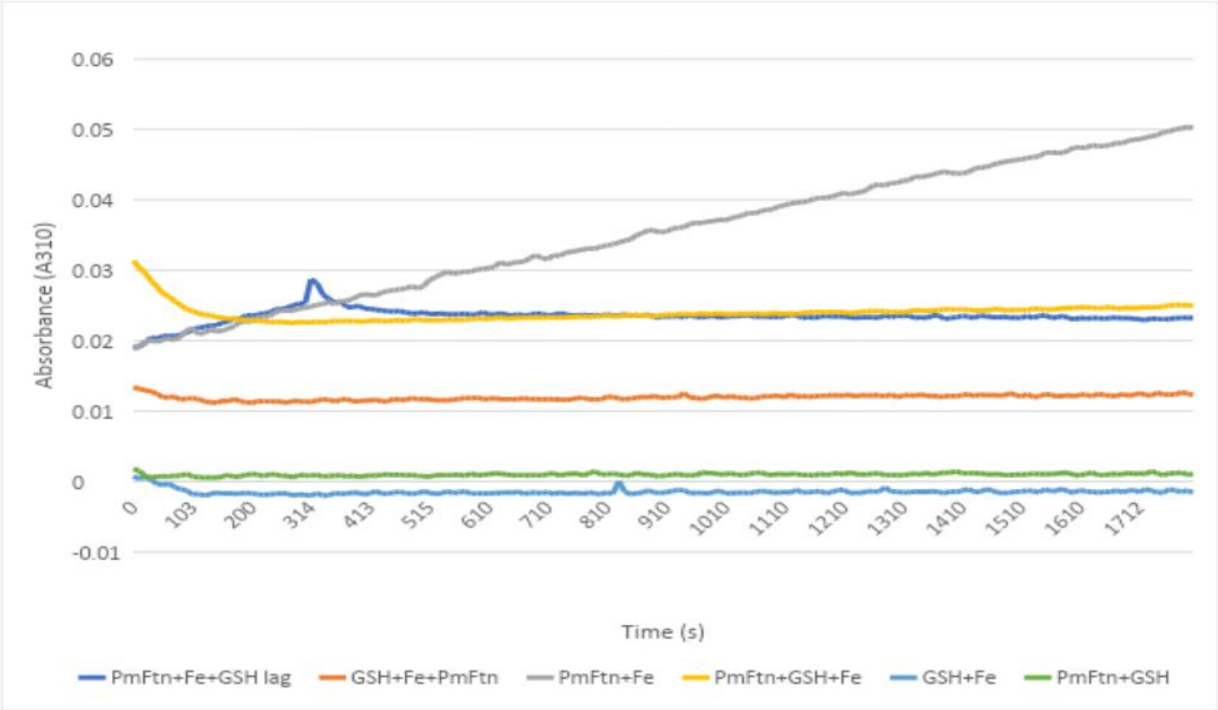

Figure 3-3. Iron mineralisation over a 30-minute time-course in the presence of PmFtn and GSH. PmFtn (0.1 µM), 50 µM ammonium ferrous sulfate, and 15 mM GSH were mixed in 50 mM MES 100 mM NaCl pH 6.5 buffer and rate of iron mineralisation was measured over 30 minutes in a spectrophotometer. The order in which reagents were added are indicated in the figure legend. PmFtn + Fe + GSH lag refers to an experiment where PmFtn alone was allowed to oxidize iron in the absence of any chelators, followed by the addition of GSH after 5 minutes. Controls included a ferritin assay in buffer alone (PmFtn + Fe), as well as the mixing of GSH and Fe (GSH + Fe) and PmFtn and GSH (PmFtn + GSH). The figure shows representative assays of three replicates.

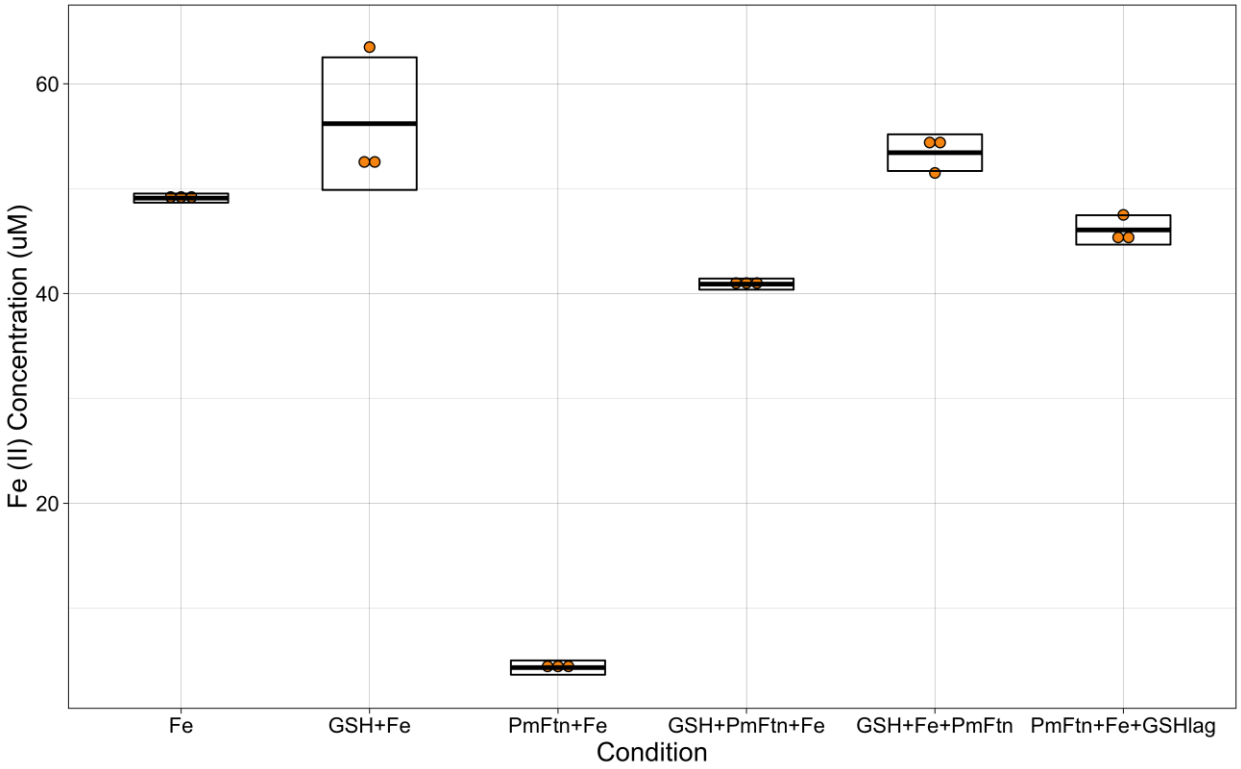

Figure 3-4. Ferrous iron remaining after 30 minutes of ferroxidase activity in the presence of GSH. 50 µM ammonium ferrous sulfate, 0.1 µM PmFtn, 15 mM GSH were mixed in 50 mM MES 100 mM NaCl pH 6.5 buffer. After 30 minutes, the amount of remaining ferrous iron was detected using a ferrozine assay by measuring absorbance at 562 nm on a spectrophotometer (extinction coefficient of 24410 $M^{-1}cm^{-1}$). Three replicates were done for each condition. The lines inside the boxes represent the mean for each experiment, and the boxes represent one standard deviation from the mean.

3.4 GSH affects initial rate of iron oxidation by PmFtn

Stopped-flow experiments were performed in the Le Brun lab at the University of East Anglia to observe the effect of GSH on the initial rapid binding and oxidation of iron at the PmFtn ferroxidase centres. When PmFtn was mixed with 96 Fe^{2+} ions in the presence of GSH, the initial absorbance at 340 nm was lower than when PmFtn was mixed with 96 Fe^{2+} ions alone, indicating lower rate of initial iron oxidation in the presence of GSH (Figure 3-5). These results indicate that while iron was still able to bind and become oxidized by PmFtn in the presence of GSH, the rate is slower than compared to when GSH was absent. In addition, the subsequent oxidation of iron in excess was found to occur at a much lower rate in the presence of GSH. When PmFtn was mixed with 96 Fe^{2+} ions in the presence of GSH, the oxidation of iron in excess of that which saturates its iron-binding sites was at a much lower rate than when PmFtn was mixed with 96 Fe^{2+}ions alone. These results support previous findings observed in the spectroscopic assays.

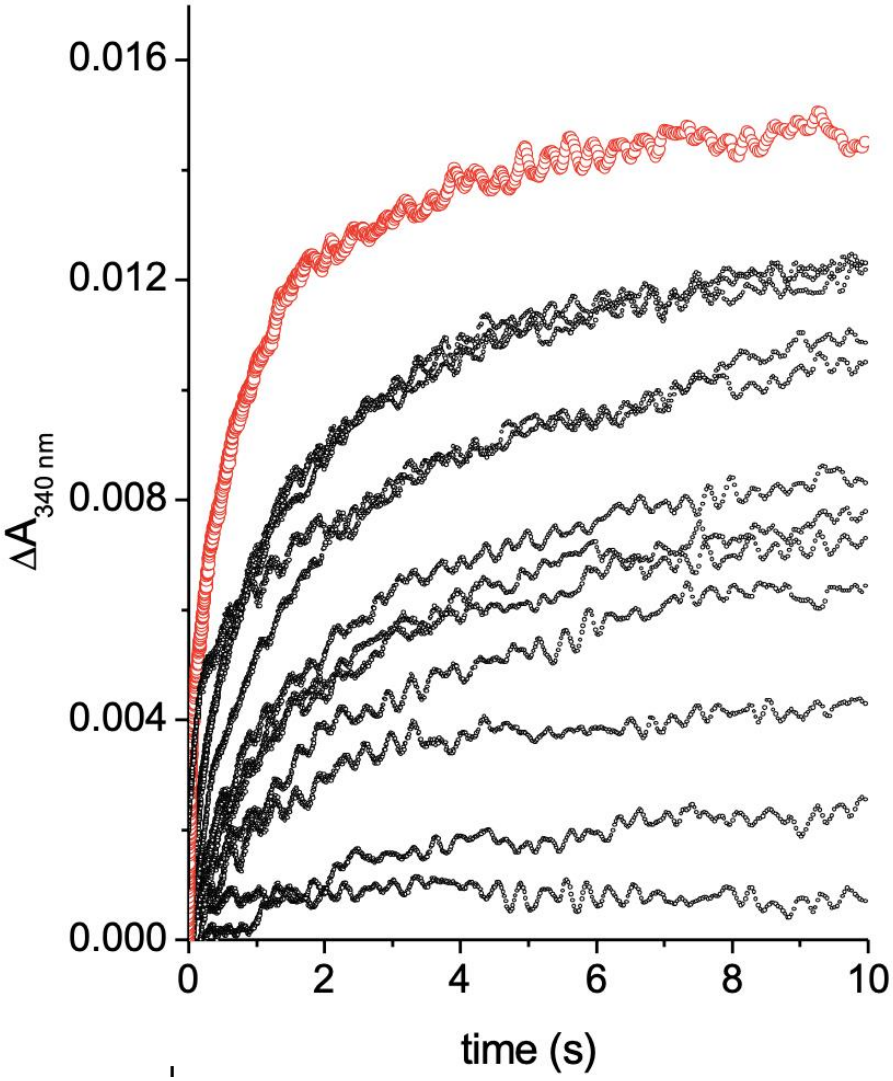

Figure 3-5. Rapid initial oxidation of iron by PmFtn is affected in the presence of GSH. Black lines indicate experiments with increasing amounts of equivalents of Fe^{2+} added, ranging from 6 ions (bottom black line) up to 96 ions (top black line). Red line indicates control experiment in which no GSH was added, with 96 ions of Fe^{2+} added.

3.5 PmFtn protects DNA from oxidative damage without binding DNA

The ability of PmFtn to protect DNA from H_2O_2 was tested to better understand the role PmFtn plays in protecting from oxidative stress. A PCR product of the ArnD gene was utilized for this study, and when run on an agarose gel alone, produced a band corresponding to ~1,200 bp. PmFtn run alone on the agarose gel produced a band corresponding to ~300 bp (Figure 3-6). PmFtn was incubated with DNA for 30 minutes in MOPS buffer at pH 7.0, and run on an agarose gel. The DNA band observed at ~1,200 bp was identical to that of DNA run alone, with a second band appearing at ~300 bp, corresponding to PmFtn (Figure 3-6). This result suggests that PmFtn does not bind DNA non-specifically. DNA was also incubated with PmFtn for 30 minutes followed by ammonium ferrous sulfate for a further 10 minutes. The mobility of the two bands was equivalent to ~1,200 bp and ~300 bp in size, suggesting that Fe^{2+} does not interact with DNA in such a way that reduces electrophoretic mobility, such as by reducing the negative charge (Figure 3-6).

DNA was incubated with ammonium ferrous sulfate for 10 minutes, followed by incubation with H_2O_2 for 5 minutes, before electrophoresis on an agarose gel. In this case, no DNA band was present on the gel, suggesting that DNA was degraded following the incubation with iron and H_2O_2 (Figure 3-6). Some material was present at the very top of the gel, likely corresponding to DNA aggregation caused by DNA damage by H_2O_2. In contrast, DNA that was incubated with PmFtn for 30 minutes and with ammonium ferrous sulfate for a further 10 minutes prior to being exposed to H_2O_2 resulted in a DNA band at ~1,200 bp, indicating that DNA was prevented from degrading (Figure 3-6).

The DNA fragment also appeared to be partially protected in the presence of GSH. DNA was incubated with ammonium ferrous sulfate for 10 minutes, and then incubated with GSH for

5 minutes before being exposed to H_2O_2 for a further 5 minutes before agarose gel electrophoresis. Under these conditions, a DNA band corresponding to ~1,200 bp was present, though at a lower intensity than the DNA-alone band (Figure 3-6). A DNA band with a mobility corresponding 1,200 bp was observed when DNA was first incubated with PmFtn for 30 minutes prior to being incubated with ammonium ferrous sulfate, GSH, and H_2O_2 (Figure 3-6). The presence of PmFtn likely sequesters ferrous iron once the GSH is oxidized by H_2O_2 increasing the mobility of the DNA.

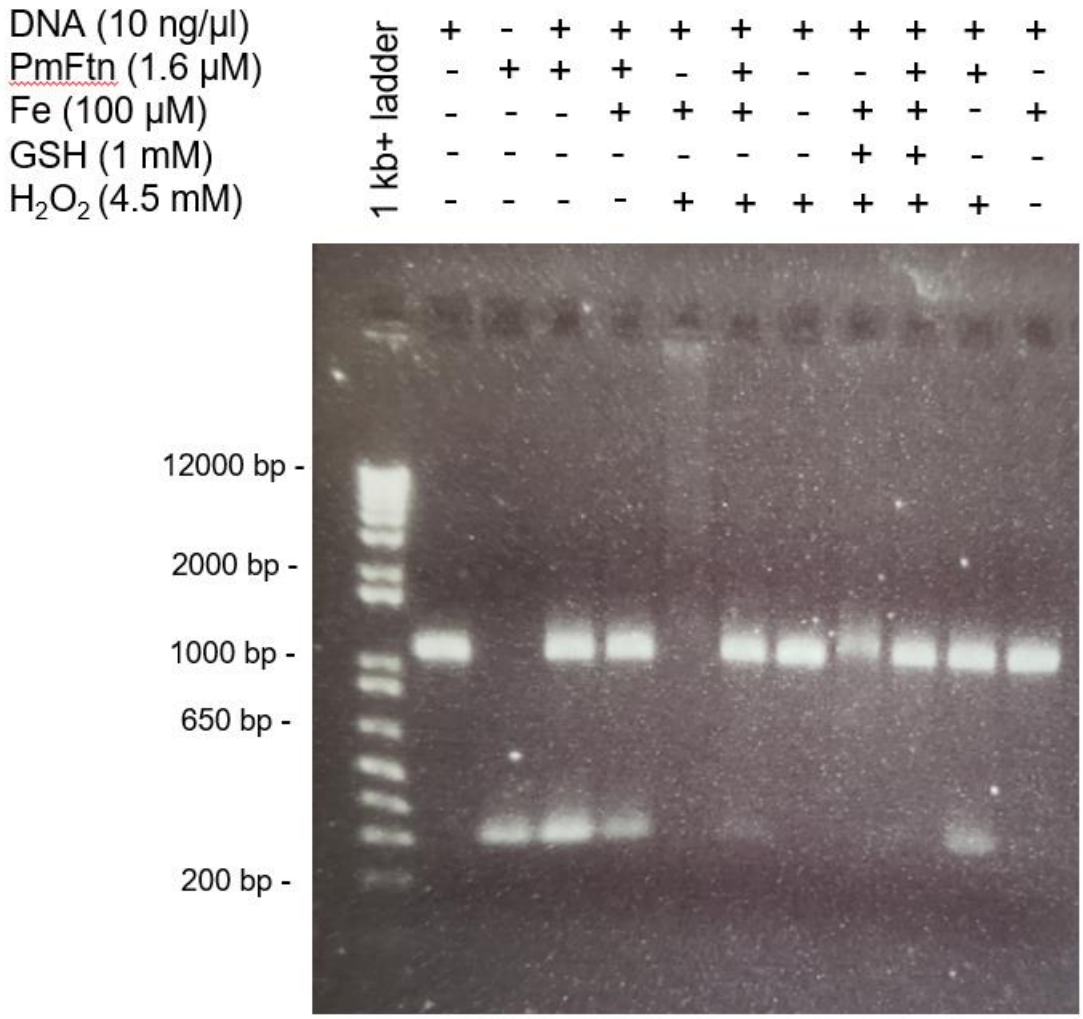

Figure 3-6. DNA is protected by PmFtn from oxidative damage. 15 ng/µL linear ArnD DNA was incubated for 30 minutes with 1.6 µM cage PmFtn protein for 30 minutes. 1 mM GSH was incubated with sample for 5 minutes. After, 100 µM ammonium ferrous sulfate was incubated with the sample for 10 minutes. Lastly, samples were subjected to an incubation with 4.5 mM H_2O_2 for 5 minutes. Samples were run on a 1% agarose gel for 30 minutes at 90 V. The gel is representative of 3 replicate experiments.

Chapter 4: Discussion

4.1 Ferroxidase activity in the presence of GSH

In a search of the literature, iron oxidation and mineralization by ferritin was assayed in the absence of biologically-relevant iron chelators which maintain the LIP. To the best of our knowledge, this study is the first to report ferritin ferroxidase activity in the presence of one of the most abundant of these biologically-relevant iron chelators, GSH. This study therefore investigates ferroxidase activity under conditions which better mimic actual cellular conditions under which ferritin would normally function.

Stopped-flow absorption spectroscopy was used to examine the rapid initial rate of iron oxidation at the ferroxidase centre, the apparent first step in the characteristic PmFtn two-step ferroxidase reaction. The results showed that in the presence of GSH, the initial rate of iron oxidation was lower than when GSH was absent (Figure 3-2). The presence of GSH at a biologically-relevant concentration competes with PmFtn to bind ferrous iron or inhibits ferroxidase activity. The presence of GSH did not completely stop iron oxidation however, as an increase in absorbance at 340 nm was recorded (Figure 3-3). The second step of PmFtn ferroxidase function, iron mineralization, was examined in the presence of GSH using spectrophotometry. In the presence of GSH, PmFtn iron mineralization was able to proceed, though at a slower rate than what was observed in the absence of GSH. Mineralization was inhibited when GSH was introduced after 5 minutes of PmFtn iron mineralization (Figure 3-3). Together with the stopped-flow results, these results indicate that PmFtn binding, oxidation, and mineralization of iron is inhibited in the presence of the biologically-relevant iron-chelator, GSH.

PmFtn rapid initial iron oxidation rates as well as mineralization rates were investigated previously using stopped-flow absorbance spectroscopy (31). In the previous study, 1 µm apo-PmFTN in 100 mM MES, pH 6.5 and 200 mM NaCl was mixed (1:1) with the 10-400 µM ferrous iron working solutions, resulting in a protein concentration of 0.5 µm during data acquisition. The buffer used in the study presented in this thesis for the measurement of the mineralization rate using spectrophotometry was 50 mM MES, pH 6.5, and 100 mM NaCl, which was mixed with 0.1 µM PmFtn and 50 µM ferrous iron. The difference in the conditions of the study presented in this thesis and that of the previous study did not appear to cause a major difference in the results obtained.

4.2 PmFtn structure and iron binding at ferroxidase centres

The crystallization conditions used in this study were based on that of a previous study, with crystals formed using hanging vapour diffusion in 0.1 M sodium acetate, pH 5.5, 1-1.2 M ammonium sulfate, and 0.9-1.2 M sodium chloride (31). PmFtn structures obtained in this study differed from PmFtn structures in the literature in both the number of molecules in the asymmetric unit and the space group. Previously, PmFtn crystals were determined to be primarily in space group P23, with only the overnight iron-soaked crystal determined to be in a different space group, $P42_12$. In this study, we reported all crystal structures to belong in space group P4, with 12 molecules in the asymmetric unit. Both the construct used in this study and that of the previous study were for a recombinant PmFtn protein which lacked the N-terminus signal peptide and plastid targeting sequence, as well as 12 amino acid residues from the C-terminus. However, the construct used in this study differed from the one used in the previous study in that it contained 3 mutations (C77V, C111V, C163V) that allowed for protein crystallization without an additional iodoacetamide treatment step.

In a previous study, PmFtn crystals had been soaked aerobically in 2 µM ammonium ferrous sulfate for 5 min., 45 min., 4 hr. and overnight (31). After 5 min., iron partially occupied site B in 6 of the 8 subunits at an occupancy between 35-50%, and solvent was modelled into the other two sites. Iron was only found in both sites A and B after 45 min, with iron occupancies at sites A and B at 75-90% and 40-50% respectively. Crystals soaked for 4 or more hours resulted in iron bound at all three iron-binding sites, as well as at two nearby sites, which are thought to be involved in nucleation of the mineral core. In this case, the iron occupancies at sites A, B and C ranging from 75-90%, 75-85%, and 40-75% respectively.

In the study presented in this thesis, PmFtn crystals were all soaked for 30 minutes, which resulted in partial occupancy at only iron-binding sites A and B for all soaking conditions. In the case of the iron-only soaked crystals, this result was different from what has been reported in the past. Iron had been previously reported to bind only site A after 45 minutes of soaking or more. However, the previous study did not perform any iron soaks at time-points between 5 min. and 45 min., so it is possible that iron binds site A between those times, as was observed in this study. The iron occupancies at sites A and B reported in this study after 30 min. for the iron-only soaks was on average 46% and 50% respectively. The average iron occupancy at site B was therefore similar to what has been previously reported. When PmFtn was soaked in the presence of both iron and GSH, the iron occupancies at both sites A and B were shown to be significantly lower than when GSH was absent, at an average of 38% and 42% respectively. This result showed that GSH was hindering iron binding at PmFtn ferroxidase centres, though not preventing it completely. When a different biologically-relevant iron chelator, cysteine, was tested during the iron soak, we were unable to show any significant difference in iron binding at

sites A and B when compared to the control. Across all soaking conditions, there was no significant difference in the iron occupancy in site A compared to the corresponding site B.

Ferrous iron binding to PmFtn was previously examined by crystallography under anaerobic conditions (31). The results from those experiments showed that iron bound only at iron-binding site A at an occupancy of ~50%, showing that dioxygen is required for iron binding at site B. In the presence of GSH, iron is observed at both sites A and B at partial occupancy. Alternatively, had GSH prevented iron binding PmFtn and halted ferroxidase activity, only solvent would be expected to be bound at the ferroxidase centres in the structure. The crystallographic results are consistent with the stopped-flow and spectroscopic assays and indicate some ferroxidase activity in the presence of GSH.

Due to limitations under which PmFtn could be crystallized, the crystallization conditions for PmFtn differed from the buffer used for the spectroscopic assays in two major ways. Firstly, the buffer used for crystallization was at a lower pH than the buffer used in the spectrophotometric assays, 5.5 and 6.5, respectively. Secondly, the ferrous iron concentration used during the PmFtn soaking experiments also differed from that of the spectroscopic assays, 2 mM and 50 µM, respectively. A higher concentration of ferrous iron was chosen for the crystal soaking experiments to provide an excess of iron to iron binding sites, to allow iron to permeate the crystals, and to overcome the possibility that some of the iron would oxidize during the soak.

4.3 The role of ferritin and GSH in diatoms

The amino acid sequence for PmFtn contains a plastid targeting sequence, suggesting the importance of PmFtn in providing iron to the iron-requiring process of photosynthesis, as well as possibly aiding in iron detoxification in the plastid. GSH is also likely located in the plastid at

high concentrations. In plant chloroplasts, GSH plays a role in maintaining a reducing environment in order to prevent the detrimental consequences of oxidative stress (68). Together, we hypothesize that GSH and PmFtn manage iron in the plastid, chelating iron and thus protecting the cell from the consequences of the Fenton reaction. The LIP located in the plastid is therefore is protected from reacting with any H_2O_2 produced during photosynthesis in the photosynthetic electron transport chain via the Mehler Reaction. The Mehler Reaction describes the photoreduction of O_2 to H_2O_2 or $O_2^{-\cdot}$, and is the most important source of H_2O_2 and ROS formation in the chloroplast (69). The DNA-protection assays (Figure 3-6) directly show that ferritin and GSH were able to protect DNA from degradation by H_2O_2. The same mechanism of protection may be at work to protect plastid DNA and other sensitive biomolecules from damage resulting from free ferrous iron.

Some marine phytoplanktonic species, including marine diatoms, exhibit what is known as diel periodicity, a light-dark cycle where certain genes are upregulated in the cell during the daylight hours, while others are upregulated during the night (63). The redox capabilities of Fe-containing metalloproteins are essential in both photosynthetic and respiratory electron transport chains (64). As such, diatoms exhibit an internal recycling of iron between metalloproteins over the diurnal cycle. This shuttling of iron between different parts of the cell poses a potential risk, as unchelated iron is liable to create ROS by reacting with H_2O_2 present in the cell. Ferritin and GSH likely play an important role managing iron as it shuttles back and forth in the cell between photosynthetic machinery employed during the daylight hours, and processes in the cell that are more active at night, such as the respiratory electron transport chain (64). Further, in the event that GSH is depleted during oxidative stress conditions in the cell, ferritin is poised to oxidize

and store iron as a ferric mineral within its inner cavity to protect the cell against ROS formation via the Fenton reaction.

4.4 Conclusions

Ferritins are important iron-storage proteins which can be found across all three domains of life, though little is understood about their function in the presence of biologically-relevant iron chelators which maintain the labile iron pool. In this study, *Pseudo-nitzchia multiseries* ferritin was biochemically and structurally characterized in the presence of the abundant biologically-relevant iron-chelator in the cell, GSH. PmFtn was shown to have ferroxidase activity in the presence of GSH. However, GSH inhibited both initial iron oxidation and mineralization rates. PmFtn ferroxidase activity was confirmed in the presence of GSH by structural characterization of the ferroxidase centre, which showed that iron was still able to bind iron-binding sites A and B. Finally, PmFtn was shown to be protective of DNA in the presence of ·OH, likely through the mode of iron detoxification and prevention of ROS formation via the Fenton reaction. The biochemical data supports a model that PmFtn and GSH function together in iron detoxification within the diatom plastid.

4.5 Future Directions

Further investigation into the relationship between ferritins, the labile iron pool, and biologically-relevant iron chelators is required. Study of the importance of ferritin in protecting the cell from oxidative stress is of particular interest, as this role is overall poorly investigated compared to role of ferritin in iron storage. PmFtn is of particular interest in regards to protecting the diatom from oxidative stress, as well as the part it plays in lending success to diatoms during iron fertilization in the ocean.

This study showed that crystallography was an effective tool for observing iron binding at PmFtn ferroxidase centres under different conditions. Future crystallography experiments could be performed to better understand the relationship between GSH and ferritin in maintaining the iron pool within the cell. Co-crystallization experiments with both PmFtn and GSH could give insight into whether they may be direct interaction between the two. In addition to this, PmFtn iron-soaking experiments could be performed in the presence of other metabolites which maintain iron in the labile iron pool, including further investigation into cysteine.

While the *in vitro* findings in this study lend evidence to the role ferritin plays in protecting against oxidative damage in the diatom cell, *in vivo* studies are required to further confirm this theory. The data point to an absence of direct binding between PmFtn and DNA, indicating that it is unlikely that PmFtn offers physical shielding of DNA as a means of protection against oxidative stress in a similar manner to Dps. An EMSA study may be performed in order to ascertain whether or not PmFtn interacts with DNA in such a way that may offer protection against oxidative stress aside from the iron detoxification method that was observed in this study.

Ferritins are ubiquitous proteins found in organisms across all domains of life. As such, any insight gained into the function of PmFtn can possibly be extended to other members of this important family of proteins.

Bibliography

1. Andrews, S. C., Robinson, A. K. & Rodríguez-Quiñones, F. Bacterial iron homeostasis. *FEMS Microbiol Rev* **27**, 215–237 (2003).

2. Bou-Abdallah, F. The iron redox and hydrolysis chemistry of the ferritins. *Biochimica et Biophysica Acta (BBA) - General Subjects* **1800**, 719–731 (2010).

3. Crichton, R. R. & Ward, R. J. Iron metabolism-new perspectives in view. *Biochemistry* **31**, 11255–11264 (1992).

4. Beinert, H., Holm, R. H. & Münck, E. Iron-sulfur clusters: nature's modular, multipurpose structures. *Science* **277**, 653–659 (1997).

5. Williams, R. J. P. & Fraústo da silva, J. J. R. Evolution was chemically constrained. *Journal of Theoretical Biology* **220**, 323–343 (2003).

6. Imlay, J. A. The molecular mechanisms and physiological consequences of oxidative stress: lessons from a model bacterium. *Nat Rev Microbiol* **11**, 443–454 (2013).

7. Wardman, P. & Candeias, L. P. Fenton chemistry: an introduction. *Radiation Research* **145**, 523–531 (1996).

8. Kakhlon, O. & Cabantchik, Z. I. The labile iron pool: characterization, measurement, and participation in cellular processes. *Free Radical Biology and Medicine* **33**, 1037–1046 (2002).

9. Yamamoto, Y. *et al.* Regulation of the intracellular free iron pool by Dpr provides oxygen tolerance to Streptococcus mutans. *J Bacteriol* **186**, 5997–6002 (2004).

10. Kumar, C. *et al.* Glutathione revisited: a vital function in iron metabolism and ancillary role in thiol-redox control. *EMBO J* **30**, 2044–2056 (2011).

11. Flohe, L. *Glutathione*. (CRC Press, 2018).

12. Rosenwasser, S. *et al.* Mapping the diatom redox-sensitive proteome provides insight into response to nitrogen stress in the marine environment. *PNAS* **111**, 2740–2745 (2014).

13. Hider, R. C. & Kong, X. L. Glutathione: a key component of the cytoplasmic labile iron pool. *Biometals* **24**, 1179–1187 (2011).

14. Lampe, R. H. *et al.* Different iron storage strategies among bloom-forming diatoms. *PNAS* **115**, E12275–E12284 (2018).

15. Morel, F. M. M. & Price, N. M. The biogeochemical cycles of trace metals in the oceans. *Science* **300**, 944–947 (2003).

16. Sarthou, G., Timmermans, K. R., Blain, S. & Tréguer, P. Growth physiology and fate of diatoms in the ocean: a review. *Journal of Sea Research* **53**, 25–42 (2005).

17. Armbrust, E. V. The life of diatoms in the world's oceans. *Nature* **459**, 185–192 (2009).

18. Groussman, R. D., Parker, M. S. & Armbrust, E. V. Diversity and evolutionary history of iron metabolism genes in diatoms. *PLoS One* **10**, (2015).

19. Marchetti, A. *et al.* Ferritin is used for iron storage in bloom-forming marine pennate diatoms. *Nature* **457**, 467–470 (2009).

20. Cohen, N. R. *et al.* Transcriptomic and proteomic responses of the oceanic diatom Pseudo-nitzschia granii to iron limitation. *Environmental Microbiology* **20**, 3109–3126 (2018).

21. Andrews, S. C. The Ferritin-like superfamily: Evolution of the biological iron storeman from a rubrerythrin-like ancestor. *Biochimica et Biophysica Acta (BBA) - General Subjects* **1800**, 691–705 (2010).

22. Harrison, P. M. & Arosio, P. The ferritins: molecular properties, iron storage function and cellular regulation. *Biochimica et Biophysica Acta (BBA) - Bioenergetics* **1275**, 161–203 (1996).

23. Bradley, J. M., Le Brun, N. E. & Moore, G. R. Ferritins: furnishing proteins with iron. *J Biol Inorg Chem* **21**, 13–28 (2016).

24. Theil, E. C. Ferritin protein nanocages use ion channels, catalytic sites, and nucleation channels to manage iron/oxygen chemistry. *Current Opinion in Chemical Biology* **15**, 304–311 (2011).

25. Chasteen, N. D. & Harrison, P. M. Mineralization in ferritin: an efficient means of iron storage. *Journal of Structural Biology* **126**, 182–194 (1999).

26. Treffry, A., Zhao, Z., Quail, M. A., Guest, J. R. & Harrison, P. M. How the presence of three iron binding sites affects the iron storage function of the ferritin (EcFtnA) of Escherichia coli. *FEBS Letters* **432**, 213–218 (1998).

27. Bauminger, E. R. *et al.* Stages in iron storage in the ferritin of Escherichia coli (EcFtnA): analysis of Mössbauer spectra reveals a new intermediate. *Biochemistry* **38**, 7791–7802 (1999).

28. Grossman, M. J., Hinton, S. M., Minak-Bernero, V., Slaughter, C. & Stiefel, E. I. Unification of the ferritin family of proteins. *Proceedings of the National Academy of Sciences* **89**, 2419–2423 (1992).

29. Baaghil, S., Lewin, A., Moore, G. R. & Le Brun, N. E. Core formation in Escherichia coli bacterioferritin requires a functional ferroxidase center. *Biochemistry* **42**, 14047–14056 (2003).

30. Calhoun, L. N. & Kwon, Y. M. Structure, function and regulation of the DNA-binding protein Dps and its role in acid and oxidative stress resistance in Escherichia coli: a review. *Journal of Applied Microbiology* **110**, 375–386 (2011).

31. Pfaffen, S., Abdulqadir, R., Le Brun, N. E. & Murphy, M. E. P. Mechanism of ferrous iron binding and oxidation by ferritin from a pennate diatom. *J Biol Chem* **288**, 14917–14925 (2013).

32. Bou-Abdallah, F. *et al.* Functionality of the three-site ferroxidase center of Escherichia coli bacterial ferritin (EcFtnA). *Biochemistry* **53**, 483–495 (2014).

33. Ebrahimi, K. H., Bill, E., Hagedoorn, P.-L. & Hagen, W. R. The catalytic center of ferritin regulates iron storage via Fe(II)-Fe(III) displacement. *Nat Chem Biol* **8**, 941–948 (2012).

34. Abdul-Tehrani, H. *et al.* Ferritin mutants of Escherichia coli are iron deficient and growth impaired, and fur mutants are iron deficient. *J Bacteriol* **181**, 1415–1428 (1999).

35. Eshelman, K. *et al.* Inhibiting the BfrB:Bfd interaction in Pseudomonas aeruginosa causes irreversible iron accumulation in bacterioferritin and iron deficiency in the bacterial cytosol. *Metallomics* **9**, 646–659 (2017).

36. Pfaffen, S. *et al.* A diatom ferritin optimized for iron oxidation but not iron storage. *J Biol Chem* **290**, 28416–28427 (2015).

37. Andrews, S. C., Smith, J. M. A., Yewdall, S. J., Guest, J. R. & Harrison, P. M. Bacterioferritins and ferritins are distantly related in evolution Conservation of ferroxidase-centre residues. *FEBS Letters* **293**, 164–168 (1991).

38. Andrews, S. C. *et al.* Site-directed replacement of the coaxial heme ligands of bacterioferritin generates heme-free variants. *J Biol Chem* **270**, 23268–23274 (1995).

39. Yasmin, S., Andrews, S. C., Moore, G. R. & Le Brun, N. E. A new role for heme, facilitating release of iron from the bacterioferritin iron biomineral. *J Biol Chem* **286**, 3473–3483 (2011).

40. Tatur, J., Hagen, W. R. & Matias, P. M. Crystal structure of the ferritin from the hyperthermophilic archaeal anaerobe Pyrococcus furiosus. *J Biol Inorg Chem* **12**, 615–630 (2007).

41. Pfaffen, S. Iron binding and oxidation by Pseudo-nitzschia multiseries ferritin. (University of British Columbia, 2014). doi:10.14288/1.0167604.

42. Michel, F. M. *et al.* The structure of ferrihydrite, a nanocrystalline material. *Science* **316**, 1726–1729 (2007).

43. Mohanty, A. *et al.* Iron mineralizing bacterioferritin A from Mycobacterium tuberculosis exhibits unique catalase-Dps-like dual activities. *Inorg Chem* **58**, 4741–4752 (2019).

44. Stookey L. L. Ferrozine---a new spectrophotometric reagent for iron. *Anal Chem* **42**, 779–781 (1970).

45. Kabsch, W. XDS. *Acta Crystallogr D Biol Crystallogr* **66**, 125–132 (2010).

46. Zwart, P. H. *et al.* Automated structure solution with the PHENIX suite. in *Structural Proteomics: High-Throughput Methods* (eds. Kobe, B., Guss, M. & Huber, T.) 419–435 (Humana Press, 2008). doi:10.1007/978-1-60327-058-8_28.

47. Vagin, A. & Teplyakov, A. MOLREP: an automated program for molecular replacement. *J Appl Cryst* **30**, 1022–1025 (1997).

48. McCoy, A. J. *et al.* Phaser crystallographic software. *J Appl Crystallogr* **40**, 658–674 (2007).

49. Emsley, P., Lohkamp, B., Scott, W. G. & Cowtan, K. Features and development of Coot. *Acta Crystallogr D Biol Crystallogr* **66**, 486–501 (2010).

50. Semsey, S. *et al.* Genetic regulation of fluxes: iron homeostasis of Escherichia coli. *Nucleic Acids Res* **34**, 4960–4967 (2006).

51. Park, S. & Imlay, J. A. High levels of intracellular cysteine promote oxidative DNA damage by driving the Fenton reaction. *Journal of Bacteriology* **185**, 1942–1950 (2003).

52. Gao, G., Li, J., Zhang, Y. & Chang, Y.-Z. Cellular iron metabolism and regulation. *Brain Iron Metabolism and CNS Diseases* (ed. Chang, Y.-Z.) 21–32 (Springer, 2019). doi:10.1007/978-981-13-9589-5_2.

53. Bou-Abdallah, F., Lewin, A. C., Brun, N. E. L., Moore, G. R. & Chasteen, N. D. Iron detoxification properties of Escherichia coli bacterioferritin. *J Biol Chem* **277**, 37064–37069 (2002).

54. Hudson, A. J. *et al.* Overproduction, purification and characterization of the Escherichia coli ferritin. *European Journal of Biochemistry* **218**, 985–995 (1993).

55. Hempstead, P. D. *et al.* Direct observation of the iron binding sites in a ferritin. *FEBS Letters* **350**, 258–262 (1994).

56. Castruita, M., Shaked, Y., Elmegreen, L. A., Stiefel, E. I. & Morel, F. M. M. Availability of iron from iron-storage proteins to marine phytoplankton. *Limnology and Oceanography* **53**, 890–899 (2008).

57. Lawson, D. M. *et al.* Solving the structure of human H ferritin by genetically engineering intermolecular crystal contacts. *Nature* **349**, 541–544 (1991).

58. Briat, J.-F., Duc, C., Ravet, K. & Gaymard, F. Ferritins and iron storage in plants. *Biochimica et Biophysica Acta (BBA) - General Subjects* **1800**, 806–814 (2010).

59. Crichton, R. R. & Declercq, J.-P. X-ray Structures of ferritins and related proteins. *Biochim Biophys Acta* **1800**, 706–718 (2010).

60. Bradley, J. M. *et al.* Reaction of O2 with a diiron protein generates a mixed-valent Fe2+/Fe3+ center and peroxide. *PNAS* **116**, 2058–2067 (2019).

61. Lawson, D. M. *et al.* Solving the structure of human H ferritin by genetically engineering intermolecular crystal contacts. *Nature* **349**, 541–544 (1991).

62. Nriagu, Jerome O., & Eric P. Skaar, eds. Trace metals and infectious diseases. MIT Press, 2015.

63. Harding, L. W. *et al*. Diel Periodicity of Photosynthesis in Marine Phytoplankton. *Marine Biology* **61**, 95-105 (1981).

64. Smith, S. R. *et al.* Transcriptional Orchestration of the Global Cellular Response of a Model Pennate Diatom to Diel Light Cycling under Iron Limitation. *PLOS Genetics* 13(3): e1006688 (2017).

65. Botebol, H. *et al.* Central role for ferritin in the day/night regulation of iron homeostasis in marine phytoplankton. *Proc Natl Acad Sci U S A* **112**, 14652–14657 (2015).

66. Hassan, H. M. & Troxell, B. Transcriptional regulation by Ferric uptake regulator (Fur) in pathogenic bacteria. *Front Cell Infect Microbiol* **3**, 59 (2013).

67. Noctor, G. & Foyer, C. H. Ascorbate and glutathione: keeping active oxygen under control. *Annual Review of Plant Physiology and Plant Molecular Biology* **49**, 249–279 (1998).

68. Yu, X. *et al.* Plastid-Localized Glutathione Reductase2–Regulated Glutathione Redox Status Is Essential for Arabidopsis Root Apical Meristem Maintenance. *The Plant Cell* **25**, 4451–4468 (2013).

69. Slesak, I., Libik, M., Karpinska, B., Karpinski, S. & Miszalski, Z. The Role of Hydrogen Peroxide in Regulation of Plant Metabolism and Cellular Signalling in Response to Environmental Stresses. *Acta Biochim Pol* **54**, 39–50 (2007).